
Rethinking Incompleteness: Formalizing Protocol Divergence and Train-Once Learning for Robust IMVC

Haolu Liu Xiyue Wang Xuanting Xie Liangjian Wen Zhao Kang

Abstract

Standard IMVC evaluation retrains separate models for different missing-data configurations. We show that this paradigm obscures a fundamental vulnerability: missing rate alone is insufficient to characterize data incompleteness. Specifically, we show that protocols with identical nominal missing rates can differ by up to $50\times$ in their proportion of fully observed samples, inducing drastically different learning regimes. We formalize this phenomenon as *incompleteness divergence*, providing measures that capture structural disparities across missing-data protocols. We further prove that for a broad class of reconstruction-based objectives, learning becomes structurally ill-posed when the proportion of complete samples falls below a critical threshold, leading to near-random performance. To bypass this theoretical bound, we propose CRAFT (Complete-data Robust Attention-masked Fusion Transformer). CRAFT shifts the burden of robustness from the loss function to the architecture via two key properties: (i) per-sample independence, which removes reliance on complete-sample co-occurrence, and (ii) mask-aware variable-length fusion, which aggregates only observed views through attention masking. This design allows a single model, trained once on complete data, to generalize to diverse missing patterns at inference time without retraining. Extensive experiments on seven benchmarks show that CRAFT matches or outperforms per-configuration baselines while reducing training overhead by $8.8\times$, demonstrating that robustness to missing data can be achieved as an inherent architectural property. Code (CRAFT) and our `imvc-audit` toolkit are available at [this link](#) and [this link](#).

1 Introduction

Real-world systems frequently capture data from diverse sensors or modalities, making multi-view representations a natural fit for complex data mining tasks. Nevertheless, the complete-data assumption underlying most multi-view clustering (MVC) methods rarely holds in practice: sensor failures, privacy constraints, and transmission errors routinely leave views unobserved for large subsets of samples [27]. This ubiquitous incompleteness has catalyzed the field of Incomplete Multi-View Clustering (IMVC).

The dominant paradigm in IMVC relies on cross-view reconstruction, where missing views are recovered to facilitate downstream clustering. Representative methods train explicit recovery modules that use complete samples as the primary source of cross-view supervision [13, 34, 5]. However, we identify two fundamental limitations in this paradigm that have been largely overlooked.

The Per-Configuration Retraining Trap. Current IMVC research evaluates each (missing-pattern, missing-rate) configuration with a separately retrained model [14, 34, 5]. This convention lacks practical justification: in real-world deployments, the missing-data distribution is often non-stationary or unknown. Treating a single deployment as multiple independent training problems is not only computationally prohibitive but also obscures the fragility of existing architectures.

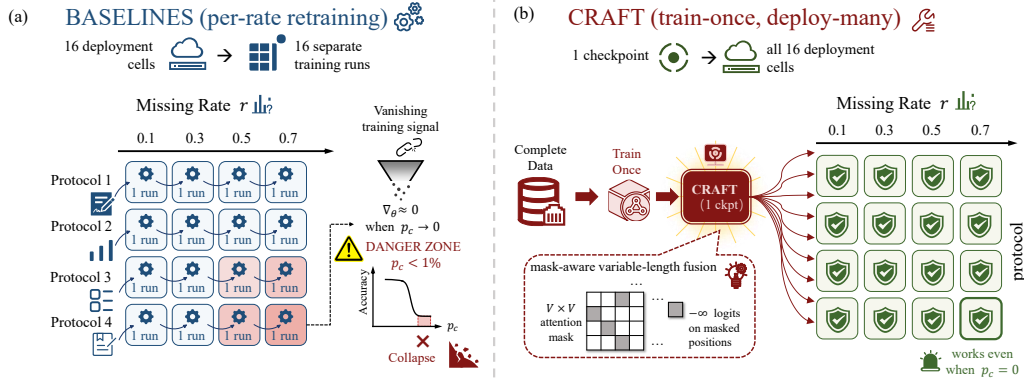


Figure 1: Per-configuration retraining vs. train-once deployment. **(a)** Baselines retrain a separate model per (protocol, r) configuration; below $p_c=1\%$ the gradient signal vanishes and training collapses. **(b)** CRAFT trains once on complete data and covers all 16 configurations (including $p_c \rightarrow 0$) via attention masking on the fusion layer—a single checkpoint replaces sixteen separate training runs.

The p_c Trainability Bound. We show that the success of reconstruction-based methods is governed by a hidden variable: the complete-sample proportion (p_c). Because reconstruction losses derive supervision primarily from cross-view co-occurrence, a low p_c starves the optimizer of gradient signals. We further show that different evaluation protocols realizing the same nominal missing rate can differ in p_c by up to $50\times$. Consequently, a method that appears robust under one protocol may collapse to near-random accuracy under another, a phenomenon we term *incompleteness divergence*. We prove that for traditional reconstruction-based objectives, this trainability collapse is structurally unavoidable.

To address these shortcomings, we propose CRAFT (Complete-data Robust Attention-masked Fusion Transformer), an architecture designed to escape this trainability bound by construction. CRAFT satisfies two structural properties. **Per-sample independence:** each sample’s representation is computed only from its observed views and shared parameters, without complete-sample co-occurrence. **Mask-aware variable-length fusion:** missing views are excluded from internal computation via attention masking rather than being zero-padded or hallucinated. This decoupling from p_c enables a “Train-Once, Deploy-Many” paradigm (Figure 1): a single CRAFT checkpoint trained on complete data covers all sixteen (protocol, r) configurations at inference.

Our main contributions are summarized as follows. **(1) Formalization of Incompleteness Divergence.** We introduce the effective missing rate (\hat{r}) and complete-sample proportion (p_c) to reveal structural disparities across IMVC protocols previously obscured by nominal missing rates. **(2) Theoretical Analysis of Collapse.** We prove that reconstruction-based learning is structurally ill-posed under low p_c , providing a rigorous explanation for why existing methods fail in sparse-data regimes. **(3) The CRAFT Architecture.** We propose a Transformer-based framework that achieves robust IMVC through per-sample independence and mask-aware fusion, eliminating the need for per-configuration retraining. **(4) Empirical Validation.** Extensive experiments on seven benchmarks demonstrate that a single CRAFT model matches or surpasses per-configuration retrained baselines while reducing training overhead by $8.8\times$.

2 Related Work

Incomplete multi-view clustering has a long pre-deep history—early methods addressed the problem through low-rank matrix factorization [12, 7, 18], incomplete multi-kernel learning [16], spectral and graph-based clustering [22, 35], and subspace alignment with missing-view inferring [25], each compensating for missing entries through a structural prior on the recovered representation. More recent deep methods inherit the cross-view supervision idea but train the representation end-to-end; we organize them by *how the supervisory signal is extracted from incomplete data* into three classes (Class 1, Class 2, Class 3 below) that match the structure of our subsequent analysis.

Class 1: cross-view reconstruction (\mathcal{F}_{rec}). The dominant paradigm trains an explicit cross-view recovery module—predicting one view from another, or reconstructing missing views from observed ones—using complete samples as the source of cross-view supervision. COMPLETER [13] and its TPAMI extension DCP [14] establish the template; subsequent methods refine the recovery mechanism through cognitive deep networks [26], contrastive multi-level feature learning [29], generative recovery via GANs and diffusion [23, 34], prototype-based imputation [11], hierarchical semantic alignment [5], attention-based partial deep clustering [30], and recent Bayesian extensions [9]. A common structural trait unites this family: the reconstruction loss is computed over pairs of views co-observed for the same sample, so the gradient flows exclusively through samples retaining at least two views. We denote this family \mathcal{F}_{rec} .

Class 2: cross-sample and distributional methods. A second class extracts supervisory signal that is not strictly per-sample: DSIMVC [19] imputes from latent-space nearest neighbors of *other* samples, DSMVC [20] reweights views to mitigate performance degradation when adding views, SURE [32] combines cross-sample contrastive alignment with noise-robust losses for partially view-aligned and sample-missing settings, and Energy-DIMC [24] aligns view distributions through energy-based models. All four compute their training signal through cross-sample or cross-view distributional relationships rather than within-sample co-observation, placing them outside the \mathcal{F}_{rec} trainability bound; their failure modes are characterized by a capability axis rather than a trainability axis.

Class 3: per-sample methods. A third class avoids cross-view reconstruction entirely: each sample’s representation is computed from its own observed views and shared parameters, with no dependence on other samples’ observation patterns. DVIMC [2] uses a variational autoencoder with a Wasserstein-barycenter mixture for per-sample latent fusion; MvCLN [31], FreeCSL [4], and I2MVC [28] similarly fuse only observed views without cross-view recovery. CRAFT belongs to this class, distinguished by attention-masked variable-length fusion. Outside clustering, attention-based fusion of observed-only modalities is established in supervised multimodal learning [17, 6], where the label Y serves as a statistical bridge that unsupervised IMVC must instead recover from cross-view co-observation alone.

3 Motivation and Insights

Notation. Given a dataset of n samples with up to V views, to be partitioned into K latent clusters $Y \in \{1, \dots, K\}$: sample i ’s feature in view- v is $x_v^{(i)} \in \mathbb{R}^{d_v}$, observed if and only if the indicator $M_v^{(i)} \in \{0, 1\}$ equals 1. We write $O_i := \{v : M_v^{(i)} = 1\}$ for sample i ’s observed-view set and call i *complete* when $|O_i| = V$. The protocol controls missingness through a single nominal rate $r \in [0, 1]$; §3.1 characterizes the realized statistics on M .

3.1 Generalized Evaluations

The two protocol-induced statistics introduced in §1—the effective missing rate \hat{r} and the complete-sample proportion p_c —admit closed forms over the mask matrix M :

$$\hat{r} = \frac{1}{nV} \sum_{i=1}^n \sum_{v=1}^V (1 - M_v^{(i)}), \quad p_c = \frac{1}{n} \sum_{i=1}^n \prod_{v=1}^V M_v^{(i)}. \quad (1)$$

Both summarize the protocol’s effect on the data but play distinct causal roles, sketched informally below.

p_c controls trainability. Methods whose training signal is computed over pairs of views co-observed within the same sample receive gradient information only from samples with $|O_i| \geq 2$. As p_c shrinks, the expected per-step gradient diminishes proportionally and training fails to converge to non-trivial accuracy.

\hat{r} controls the capability ceiling. Even a perfectly trained method is bounded by the information available in observed views, and that bound depends on view–sample coverage, summarized by \hat{r} . The two axes are independent: two protocols on the same dataset can share \hat{r} (identical capability ceiling) yet differ substantially in p_c (different trainability). We refer to the joint (\hat{r}, p_c) characterization as *incompleteness divergence*, since two protocols realizing the same nominal r may diverge sharply along either axis.

Table 1: Four evaluation protocols and their limiting hidden variables (\hat{r} , p_c) as $n \rightarrow \infty$. Protocols 1–2 keep p_c moderate (lenient regime); Protocols 3–4 drive $p_c \rightarrow 0$ (stringent regime). V is the total view count and r the nominal missing rate.

Protocol	Mechanism	Granularity	\hat{r}	p_c
1	Sample-level deletion (protected)	sample	r/V	$1 - r$
2	Entry-wise Bernoulli (protected)	entry	r/V	$(1 - r/(V-1))^{V-1}$
3	Per-view independent (one-hot)	entry	$r - r^V/V$	$(1 - r)^V$
4	Entry-wise Bernoulli (protected, V -scaled)	entry	$\min(r, (V-1)/V)$	$\max(0, (1 - Vr/(V-1))^{V-1})$

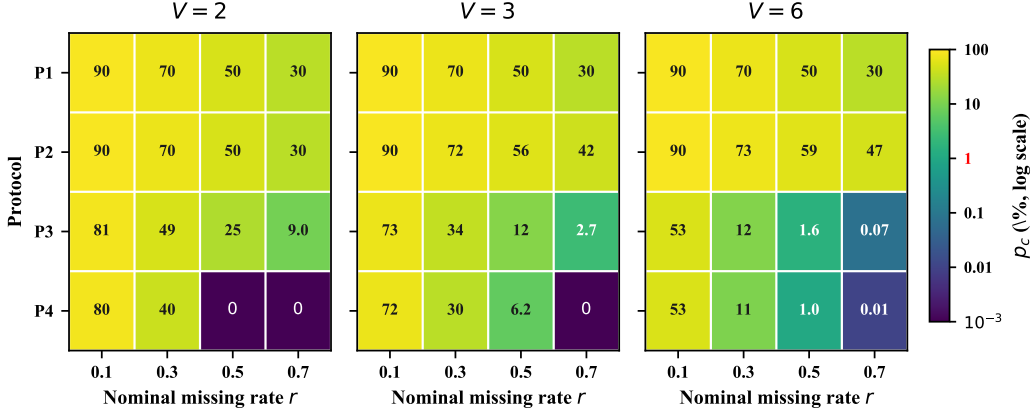


Figure 2: Complete-sample proportion p_c (% , log color scale) under the four protocols, across $V \in \{2, 3, 6\}$ and $r \in \{0.1, 0.3, 0.5, 0.7\}$. The 1% tick (red) on the colorbar marks the trainability boundary: every \mathcal{F}_{rec} method drops to near-random accuracy below it.

3.2 Four Evaluation Protocols and Up-to-50 \times Divergence in p_c

Existing IMVC protocols (Protocols 1 and 2) reach low p_c only at very low effective missing rates ($\hat{r} \leq 1/V$)—for instance, Protocol 1 at $r=1$ pins \hat{r} to $1/V \approx 16.67\%$ on $V=6$. This \hat{r} range is too narrow for current evaluations to reach the $p_c < 1\%$ regime where \mathcal{F}_{rec} trainability is at stake. We therefore introduce two complementary new protocols: Protocol 3 uses per-view independent masking with a one-hot guarantee, letting p_c decay as $(1 - r)^V$ while \hat{r} rises with r ; Protocol 4 uses entry-wise Bernoulli masking with parameters chosen to drive p_c to zero. The two masking mechanisms are independent; a single new protocol cannot cover both.

Three orthogonal design choices distinguish the protocols used in the IMVC literature [13, 14, 5]:

- *Granularity*: whether masking decisions are made per sample (delete entire view-subsets from selected samples) or *entry-wise* (delete each entry of M independently);
- *Protected view*: whether each sample retains at least one view by construction (some implementations enforce a “protected view”; others allow $|O_i| = 0$);
- *One-hot guarantee*: whether at least one view of each sample is guaranteed observed via an explicit constraint, rather than as a statistical consequence of the masking distribution.

These choices yield four canonical protocols (Table 1), summarized by their limiting \hat{r} and p_c as $n \rightarrow \infty$ (derivations in Appendix C.1, Monte Carlo verification in Appendix C.2):

What drives the divergence. Two compounding asymmetries make the four protocols realize sharply different p_c at the same nominal r : entry-wise Bernoulli masking (Protocols 2–4) drives p_c as a power of V , while a per-sample protection clause (Protocols 1 and 2) keeps every sample with at least one observed view in expectation. The result, visible in Figure 2, partitions the family into a *lenient* regime (Protocols 1, 2; $p_c \geq 30\%$ throughout) and a *stringent* regime (Protocols 3, 4), with worst-case spread $\sim 50\times$ at $V=6, r=0.5$.¹

Coverage gap. All nine audited IMVC implementations (Appendix C.4) realize protocols with $p_c \geq 50\%$ at $r=0.5, V=6$. To our knowledge, no prior evaluation tests the $p_c \lesssim 1\%$ regime where

¹The 50 \times phenomenon emerges only at $V \geq 3$ and moderate-to-high r ; at $V=2$ or $r \leq 0.1$ the four protocols produce nearly identical p_c .

\mathcal{F}_{rec} trainability collapses—the regime emerging under entry-wise missingness without protection. CRAFT escapes this dependence by construction and is excluded from the audit.

4 Theoretical Analysis

We formalize two architectural conditions on the encoder f_θ that produces fused representations $h^{(i)} = f_\theta(\{x_v^{(i)}\}_{v \in O_i}) \in \mathbb{R}^d$ from observed views, and state the resulting trainability bound; the per-sample loss is $\mathcal{L}(\theta) = \frac{1}{n} \sum_i \ell(h^{(i)}, x^{(i)})$. Full SGD-trajectory notation and theorem proofs appear in Appendix B.

Condition C1 (Per-sample independence). $h^{(i)}$ depends only on sample i 's observed views and shared parameters; the training loss has no cross-sample terms and no dependence on the observation patterns of other samples.

Condition C2 (Mask-aware variable-length fusion). f_θ is defined for any subset $O_i \subseteq \{1, \dots, V\}$ with $|O_i| \geq 1$, producing $h^{(i)}$ via a mechanism that excludes missing views from internal computation rather than zero-padding their inputs into a fixed-cardinality structure.

Assumption 4.1 (Conditional independence given Y). *With X_v denoting the random variable underlying $x_v^{(i)}$, $P(X_1, \dots, X_V | Y) = \prod_{v=1}^V P(X_v | Y)$.*

Throughout, \mathcal{F}_{rec} denotes the Class 1 reconstruction family of §2. We first state a universal capability bound that applies to every method regardless of architecture; the trainability results that follow are distribution-free, with Assumption 4.1 required only by the second inequality of Theorem 4.1.

Theorem 4.1 (Capability bound). *For any clustering function taking observed views $S \subseteq \{1, \dots, V\}$ as input, the bound*

$$\max_{v \in S} I(X_v; Y) \leq I(\{X_v\}_{v \in S}; Y)$$

holds unconditionally. Under Assumption 4.1, the additional bound $I(\{X_v\}_{v \in S}; Y) \leq \sum_{v \in S} I(X_v; Y)$ also applies (proof in Appendix B.2).

Theorem 4.1's second inequality, the capability ceiling, applies regardless of architecture: when individual views carry little information about Y , the joint mutual information is bounded by their sum (Assumption 4.1) and caps achievable accuracy independently of trainability, which can explain a $V=3$ MultiFashion collapse for methods outside \mathcal{F}_{rec} (e.g., Energy-DIMC).

Proposition 4.1 (Trainability bound for \mathcal{F}_{rec}). *For any loss $\ell \in \mathcal{F}_{rec}$ and protocol P , $\|\mathbb{E} \nabla_\theta \mathcal{L}\| \leq C_g \cdot q_2(P)$, where $q_2(P) = \mathbb{P}_{M \sim P}[|O| \geq 2]$ and C_g is the per-sample gradient bound (full statement and proof in Appendix B.1).*

For strict-complete \mathcal{F}_{rec} training, $q_2(P)$ reduces to p_c ; the gradient signal vanishes as $p_c \rightarrow 0$, predicting near-random accuracy below a critical p_c threshold.

Theorem 4.2 (Family-local necessity within \mathcal{F}_{rec}). *For protocols P_1, P_4 at the same nominal rate r with $q_2(P_1)$ above threshold and $q_2(P_4) \rightarrow 0$, the expected cross-protocol accuracy gap of any method using $\ell \in \mathcal{F}_{rec}$ is bounded below by an explicit threshold depending only on optimizer step size, training budget, and C_g (formal ϵ -stability statement and proof in Appendix B.3).*

This makes any cross-protocol collapse within \mathcal{F}_{rec} structural rather than a tuning artifact. The result is *family-local*: distributional and cross-sample methods (e.g., Energy-DIMC) are out of scope for the trainability bound and are instead bounded by the capability ceiling (Theorem 4.1).

Corollary 4.1 (Sufficiency of C1+C2). *Any method satisfying C1 and C2 escapes Proposition 4.1's trainability constraint; its accuracy is bounded only by the capability ceiling (Theorem 4.1).*

5 CRAFT

CRAFT instantiates the two conditions of §4: C1 via complete-data training with per-view reconstruction targets, and C2 via a Transformer with attention masking [21, 17] that admits variable-length input in the spirit of Set Transformer [10] and Perceiver [8], specialized to unsupervised

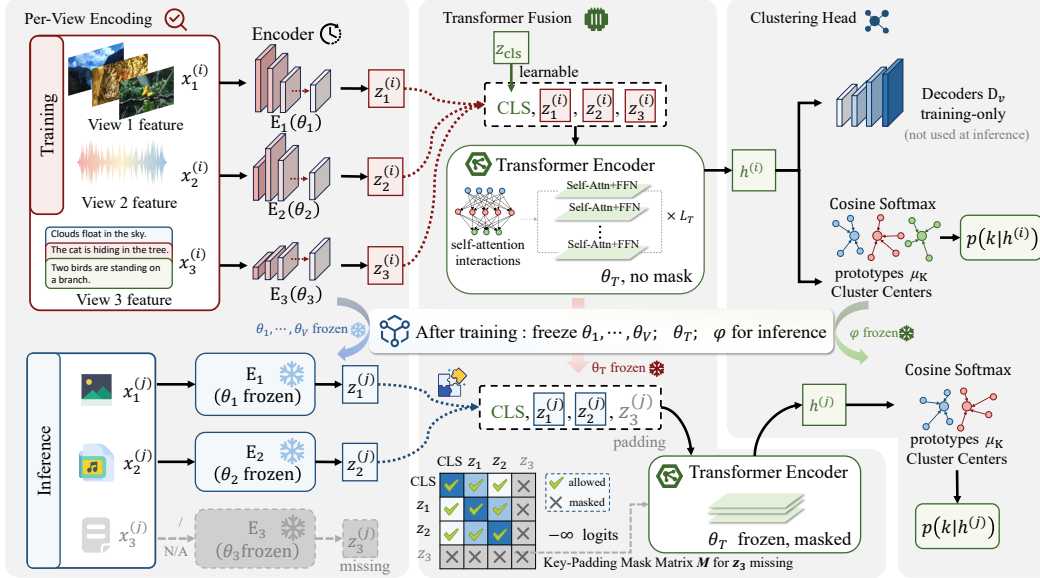


Figure 3: CRAFT architecture: per-view encoders, Transformer fusion with a learnable [CLS] token, and a cosine softmax cluster head. **Top:** complete-data training. **Bottom:** inference under missing views (z_3 missing shown) via key-padding mask. The depicted modalities ($V=3$, image/audio/text) and the masked-out view are illustrative only; CRAFT supports arbitrary view types and arbitrary missing patterns at inference. Hyperparameters in Appendix A.2.

IMVC. By embedding robustness in the architecture rather than the loss, CRAFT escapes the trainability bound of Proposition 4.1 by construction (Corollary 4.1).

We distinguish two tiers. **CRAFT-Core** is the C1+C2-mandated minimum—Stage 1 reconstruction, cosine cluster head, and attention masking—sufficient to escape Theorem 4.2. **CRAFT** (canonical) adds consistency loss, masked fine-tuning, entropy and KL regularizers, and Stage 2 fine-tuning to approach the capability ceiling (Theorem 4.1), particularly at high V with few observed views (Figure 3; ablation in Appendix E.2).

5.1 Transformer Architecture

Per-view encoding. View-specific MLP encoders E_v map each view to a shared d -dimensional embedding $z_v^{(i)} = E_v(x_v^{(i)}) \in \mathbb{R}^d$. A learnable [CLS] token is prepended to the sequence of view embeddings, yielding $[[\text{CLS}], z_1^{(i)}, \dots, z_V^{(i)}]$ for each sample.

Masked self-attention. A Transformer block with multi-head self-attention is applied to the token sequence. For sample i at evaluation time with observed-view set $O_i \subseteq \{1, \dots, V\}$, the key-padding mask is set so that positions corresponding to $v \notin O_i$ receive attention logit $-\infty$. The softmax denominator excludes these positions, ensuring missing views contribute exactly zero to the attention weights and to the resulting fused representation (Appendix B.5). The [CLS] token’s output $h^{(i)}$ serves as the fused sample representation.

Cluster head. A cosine softmax classifier maps the fused representation $h^{(i)}$ to a soft cluster assignment over K clusters. The classifier weights are L_2 -normalized prototypes; classification logits are scaled cosine similarities.

5.2 Two-Stage Training on Complete Data

CRAFT trains in two stages, both applied to complete samples (no masked positions). The inference-time mask is applied only at evaluation—a train/inference asymmetry that realizes Corollary 4.1 in practice.

Stage 1: representation learning. The Stage 1 loss combines a per-view reconstruction term and a cross-view consistency term:

$$\mathcal{L}_{\text{stage1}}(\theta) = \underbrace{\frac{1}{n} \sum_{i=1}^n \sum_{v=1}^V \|D_v(h^{(i)}) - x_v^{(i)}\|^2}_{\mathcal{L}_{\text{recon}}} + \lambda_{\text{repr}} \mathcal{L}_{\text{repr}}(\{z_v^{(i)}\}_v), \quad (2)$$

where D_v is a view-specific decoder MLP and $\mathcal{L}_{\text{repr}}$ is a SimSiam-style consistency loss on the per-view embeddings of the same sample [3] (formal definitions: Appendix A.6). Both terms are per-sample, satisfying C1 by construction; because training uses only complete samples, the gradient is independent of the inference-time protocol’s p_c . Predicting each view from the fused representation maximizes a lower bound on cluster-relevant information $I(h; Y)$ under Assumption 4.1 (Appendix B.4).

Stage 2: cluster fine-tuning. The Stage 1 representation is not cluster-aligned by default: h captures multi-view structure, but its geometry need not place samples of the same cluster close to one another. Stage 2 adds a cluster head g_ϕ and a clustering objective:

$$\mathcal{L}_{\text{stage2}}(\theta, \phi) = \mathcal{L}_{\text{cluster}}(g_\phi(h^{(i)})) + \beta \mathcal{L}_{\text{ent}} + \gamma \mathcal{L}_{\text{KL}}, \quad (3)$$

Here $\mathcal{L}_{\text{cluster}}$ is a self-labeled cross-entropy on cosine softmax outputs with epoch-refreshed pseudo-labels, \mathcal{L}_{ent} is an anti-collapse entropy regularizer on batch-averaged predictions, and \mathcal{L}_{KL} enforces consistency between predictions from MFT-sampled view-subsets (§5.3); $\gamma=0$ when MFT is disabled (formal definitions: Appendix A.6; full procedure: Algorithm 1, Appendix A.5). All three terms are per-sample, preserving C1.

5.3 Masked Fine-Tuning

Stage 2 optionally applies *masked fine-tuning* (MFT): for each sample in each batch, draw $k \sim \text{Uniform}(\{0, \dots, V - 2\})$ and randomly exclude k views via the same key-padding mask used at inference. This aligns the Stage 2 training distribution with the inference-time mask patterns and acts as a view-subset ensemble (Appendix B.6). MFT helps with $V \geq 3$ where multiple non-empty subsets exist; on $V = 2$, only the full-view subset contributes and MFT degrades to noise injection.

6 Experiments

Our experiments answer four questions in turn: (i) do \mathcal{F}_{rec} baselines collapse where Theorem 4.2 predicts? (ii) is the collapse uniform across V and across distinct recovery mechanisms? (iii) does a single CRAFT checkpoint match per-configuration retrained baselines, and at what cost? (iv) which CRAFT components carry the load? Cross-protocol comparison (§6.2) addresses (i)–(iii); the component ablation (§6.3) addresses (iv).

6.1 Setup

Baselines and protocol grid. We evaluate CRAFT against the three classes of §2: Class 1 (COMPLETER [13], DCP [14], DCG [34], HSACC [5]), Class 2 (Energy-DIMC [24]), and Class 3 (DVIMC [2]), across the protocol-rate grid of §3.2. Three datasets are reported in the main text; four more, along with hyperparameters, hardware, seed protocol, and ACC/NMI/ARI metric details, appear in Appendix A.1. “CRAFT” refers throughout to the canonical configuration of §5.

Training fairness. Every \mathcal{F}_{rec} baseline is retrained per configuration with the test-time missing distribution as its training distribution—a transductive advantage CRAFT does not receive, since CRAFT trains once on complete data only. To verify that CRAFT’s stability is architectural rather than a data-distribution artifact, we additionally train CRAFT under each configuration’s missing distribution; the gap to the complete-trained variant stays below 3% on tested configurations (Appendix D.6). The comparison is therefore biased *toward* the baselines if anything.

6.2 Cross-Protocol Comparison

\mathcal{F}_{rec} baselines collapse uniformly at $p_c < 1\%$, as Theorem 4.2 predicts. Table 2 reports clustering accuracy across the sixteen (protocol, r) configurations per dataset, with methods grouped

Table 2: Clustering accuracy (%) under Protocol 1 (lenient) and Protocol 4 (stringent). Within each dataset, methods are grouped by class: \mathcal{F}_{rec} (DCG, COMPLETER, DCP, HSACC), cross-sample (Energy-DIMC), and per-sample (DVIMC, CRAFT). Baselines retrain 16 models per dataset (one per (P, r) configuration); CRAFT* uses a **single checkpoint** per dataset for all 16 configurations. Bold/underline = best/second per column; ‡ $\leq 40\%$ on $K=10$; — = method failure (initialization crash or data-loader runtime error). † on a method name = single-seed evaluation; all other methods are 5-seed mean.

Method	Protocol 1 ($p_c \gg 0$)				Protocol 4 ($p_c \approx 0$)			
	0.1	0.3	0.5	0.7	0.1	0.3	0.5	0.7
<i>CUB</i> ($V=2, K=10$)								
DCG [34]	71.50	<u>72.56</u>	<u>73.33</u>	63.50	70.28	65.39	15.61‡	17.72‡
COMPLETER [13]	51.33	61.60	49.83	18.90‡	61.23	18.27‡	36.43‡	36.43‡
DCP [14]	65.00	57.50	51.33	26.00‡	64.17	29.67‡	36.83‡	36.83‡
HSACC [5]	63.13	54.00	43.40	29.67‡	59.50	33.13‡	38.63‡	38.63‡
Energy-DIMC [24]	<u>75.20</u>	67.77	58.20	51.56	<u>71.29</u>	53.52	<u>42.38</u>	<u>42.38</u>
DVIMC† [2]	22.67‡	27.67‡	22.67‡	22.67‡	19.83‡	26.17‡	—	—
CRAFT*	82.09	79.19	76.04	73.61	80.89	74.15	68.99	68.99
<i>HandWritten</i> ($V=6, K=10$)								
DCG†	68.50	79.25	62.25	62.30	65.25	32.60‡	14.45‡	12.75‡
COMPLETER	92.15	67.61	89.51	75.25	85.06	89.31	58.34	12.65‡
DCP	82.35	83.90	80.00	71.55	82.10	24.60‡	18.15‡	16.25‡
HSACC	76.53	87.91	87.10	80.56	89.39	15.05‡	14.24‡	13.52‡
Energy-DIMC	<u>96.65</u>	<u>96.37</u>	<u>96.09</u>	<u>96.37</u>	<u>96.09</u>	<u>94.87</u>	<u>92.75</u>	<u>83.26</u>
DVIMC†	37.30‡	84.05‡	79.55	24.30‡	71.40	20.00‡	77.05	—
CRAFT*	97.60	97.57	97.57	97.58	97.53	96.82	93.69	85.21
<i>MultiFashion</i> ($V=3, K=10$)								
DCG†	96.29	91.99	85.65	76.25	91.70	71.78	48.22	11.68‡
COMPLETER	79.92	87.23	90.66	<u>90.09</u>	83.08	87.87	46.37	—
DCP	86.04	72.75	72.26	68.95	75.24	67.21	69.36	25.11‡
HSACC	97.46	96.40	<u>91.67</u>	83.36	94.34	82.50	49.80‡	21.61‡
Energy-DIMC	<u>93.30</u>	91.64	90.19	89.90	91.97	<u>88.53</u>	79.77	29.14‡
DVIMC	83.86	86.62	88.82	87.21	86.65	84.09	<u>80.43</u>	—
CRAFT*	93.21	<u>92.82</u>	92.44	91.97	<u>92.73</u>	90.83	88.12	85.41

into the three classes of §2. No strict-complete \mathcal{F}_{rec} baseline (DCP, DCG, COMPLETER, HSACC) on a $K=10$ benchmark exceeds 40% accuracy in the stringent regime, while CRAFT consistently retains accuracy above 65%. The collapse is structural rather than a tuning artifact (Appendix A.4), confirming the gradient-counting prediction of Proposition 4.1 and Theorem 4.2. The transition is phase-like rather than gradual: \mathcal{F}_{rec} methods either receive enough pairwise-observation signal to converge or fail to differentiate from random initialization, with no intermediate regime accessible through tuning. The binary character follows directly from Proposition 4.1’s bound being multiplicative in $q_2(P)$, so the gradient signal collapses rather than degrades (Appendix D). These results confirm that \mathcal{F}_{rec} trainability is governed by p_c alone, as Theorem 4.2 predicts.

Trainability and capability are two distinct failure modes, conflated by prior evaluations. A controlled isolation configuration on HandWritten—Protocol 1 at $r=1$, giving $\hat{r}=1/V$ and $p_c = 0$ exactly—confirms p_c as the causal driver rather than a correlate of \hat{r} : \mathcal{F}_{rec} baselines collapse as predicted, while both CRAFT-Core and canonical CRAFT retain above 89% accuracy without re-training (Appendix D.9). Energy-DIMC’s preserved accuracy at vanishing p_c reflects its position outside \mathcal{F}_{rec} . On the $V=3$ MultiFashion dataset at the most stringent rate it nonetheless collapses; this is the information-theoretic capability ceiling (Theorem 4.1), not a training failure. CRAFT, satisfying C1 and C2, clears the same ceiling under the same conditions. Two distinct failure modes are at work in IMVC, conflated by prior evaluations: *trainability failure* (gradient signal vanishes; addressable by escaping \mathcal{F}_{rec}) and *capability failure* (information-theoretic limit; addressable only by accessing more views). CRAFT-Core, the bare C1+C2 minimum without engineering refinements, already escapes the trainability bound; engineering closes the gap to canonical CRAFT by improving extraction efficiency under the capability ceiling, rather than addressing the trainability bound itself (Appendix E.1). This dichotomy validates the C1+C2 framework: trainability is architecturally escapable, while capability remains data-bound (Theorem 4.1).

Baseline failure is method-invariant within \mathcal{F}_{rec} , while a single CRAFT checkpoint covers all sixteen configurations at $8.8\times$ lower training cost. HSACC’s accuracy on MultiFashion swings by 76% between the lenient and stringent regime endpoints; the pattern is method-invariant within \mathcal{F}_{rec} , with every evaluated baseline collapsing by tens of points on at least one dataset’s stringent regime regardless of recovery mechanism—contrastive prediction (COMPLETER, DCP), diffusion generation (DCG), or hierarchical alignment (HSACC) alike. The uniformity argues that the bottleneck is the loss family itself rather than its instantiations: further refinements within \mathcal{F}_{rec} would re-encounter the same bound (Appendix D). Per-configuration tuning gives baselines a narrow edge at individual lenient configurations (Table 2); CRAFT trades this small lenient-cell margin for stability across the entire (protocol, r) grid. A single CRAFT checkpoint covers all sixteen configurations per dataset at $8.8\times$ lower wall-clock cost than the strongest baseline’s per-configuration retraining (Appendix D.8); the rate-matched control in §6.1 confirms this advantage is architectural (Appendix D.6).

The collapse is universal across $V \in \{2, 3, 6\}$, ruling out V -specific artifacts. \mathcal{F}_{rec} baselines retreat to a dataset-specific floor whenever $p_c \rightarrow 0$, with the absolute floor depth varying by dataset (capability is shaped by view information density) but the trigger remaining uniformly p_c . This empirically anchors Theorem 4.2’s family-local guarantee against V -specific artifacts— p_c remains the decisive trainability variable across the grid (Appendix D).

6.3 Component Ablation

The reconstruction loss carries the Stage 1 load; Stage 2 components contribute marginally. A subtractive ablation under Protocol 4 yields three qualitative findings; per-rate numbers appear in Appendix E.1. The reconstruction loss is the load-bearing Stage 1 signal: consistency-only training collapses to near-random, and skipping Stage 1 entirely degrades accuracy by 20–31% across rates. Stage 2 components contribute only marginally—removing the cluster-head fine-tuning or the entropy regularizer leaves accuracy within one point of canonical. The consistency loss and masked fine-tuning are both V -dependent, helping at $V \geq 3$ but degrading at $V=2$; CRAFT therefore enables both only at $V \geq 3$ by default. These findings confirm that C1+C2 is the trainability-relevant core: engineering refinements only sharpen extraction efficiency under the capability ceiling, leaving the trainability bound already escaped by reconstruction alone.

CRAFT-Core, the bare C1+C2 minimum, escapes the trainability bound at every configuration. CRAFT-Core with all engineering components removed exceeds every \mathcal{F}_{rec} baseline on both tested datasets, but trails canonical CRAFT by $\sim 2\%$ on CUB and up to $\sim 32\%$ on HW under $V=6$, $r=0.7$, where masked fine-tuning carries the capability load (Appendix E.2). A four-hyperparameter sensitivity sweep (Appendix E.3) confirms canonical CRAFT is robust within the recommended ranges. These results confirm Corollary 4.1: C1+C2 is sufficient for trainability, and capability gains trace cleanly to identifiable engineering components rather than to opaque interactions.

7 Conclusion

We introduced CRAFT, an architecture that shifts robustness from the loss function to the model structure. We prove that reconstruction-based methods are structurally bounded by the complete-sample proportion (p_c), making the current “per-configuration” retraining paradigm fragile. By satisfying per-sample independence and mask-aware fusion, CRAFT escapes this bound. A single CRAFT checkpoint trained on complete data generalizes across the entire (protocol, r) grid, matching specialized baselines while reducing training overhead by $8.8\times$. Our work suggests that future IMVC research should report p_c as a standard metric and prioritize architectural refinements over algorithmic recovery. The limitation of CRAFT is that it only focuses on the cross-view reconstruction loss family in unsupervised IMVC. Extending the C1+C2 design to supervised multi-view classification or other multi-modal learning settings can be explored in the future.

References

- [1] Shai Ben-David, John Blitzer, Koby Crammer, Alex Kulesza, Fernando Pereira, and Jennifer Wortman Vaughan. A theory of learning from different domains. *Machine Learning*, 79(1-2):151–175, 2010.

- [2] Wenlan Chen, Lu Gao, Cheng Liang, and Fei Guo. Deep variational incomplete multi-view clustering with information-theoretic guidance. In *Proceedings of the 33rd ACM International Conference on Multimedia (MM '25)*, pages 2457–2466. ACM, 2025.
- [3] Xinlei Chen and Kaiming He. Exploring simple siamese representation learning. In *Proceedings of the IEEE/CVF Conference on Computer Vision and Pattern Recognition (CVPR)*, pages 15750–15758, 2021.
- [4] Yuzhuo Dai, Jiaqi Jin, Zhibin Dong, Siwei Wang, Xinwang Liu, En Zhu, Xihong Yang, Xinbiao Gan, and Yu Feng. Imputation-free and alignment-free: Incomplete multi-view clustering driven by consensus semantic learning. In *Proceedings of the IEEE/CVF Conference on Computer Vision and Pattern Recognition (CVPR)*, pages 5071–5081, 2025.
- [5] Xiaojian Ding, Lin Zhao, Xian Li, and Xiaoying Zhu. Incomplete multi-view clustering via hierarchical semantic alignment and cooperative completion. In *Advances in Neural Information Processing Systems (NeurIPS)*, 2025.
- [6] Kaiming He, Xinlei Chen, Saining Xie, Yanghao Li, Piotr Dollár, and Ross Girshick. Masked autoencoders are scalable vision learners. In *Proceedings of the IEEE/CVF Conference on Computer Vision and Pattern Recognition (CVPR)*, pages 16000–16009, 2022.
- [7] Menglei Hu and Songcan Chen. Doubly aligned incomplete multi-view clustering. In *Proceedings of the Twenty-Seventh International Joint Conference on Artificial Intelligence (IJCAI)*, pages 2262–2268, 2018.
- [8] Andrew Jaegle, Felix Gimeno, Andrew Brock, Andrew Zisserman, Oriol Vinyals, and João Carreira. Perceiver: General perception with iterative attention. *arXiv preprint arXiv:2103.03206*, 2021.
- [9] Jiaqi Jin, Siwei Wang, Zhibin Dong, Xihong Yang, Xinwang Liu, En Zhu, and Kunlun He. Deep incomplete multi-view clustering with distribution dual-consistency recovery guidance. In *Proceedings of the IEEE/CVF International Conference on Computer Vision (ICCV)*, pages 1016–1026, 2025.
- [10] Juho Lee, Yoonho Lee, Jungtaek Kim, Adam Kosiorek, Seungjin Choi, and Yee Whye Teh. Set transformer: A framework for attention-based permutation-invariant neural networks. In *International Conference on Machine Learning (ICML)*, pages 3744–3753, 2019.
- [11] Haobin Li, Yunfan Li, Mouxing Yang, Peng Hu, Dezhong Peng, and Xi Peng. Incomplete multi-view clustering via prototype-based imputation. In *Proceedings of the Thirty-Second International Joint Conference on Artificial Intelligence (IJCAI)*, pages 3911–3919, 2023.
- [12] Shao-Yuan Li, Yuan Jiang, and Zhi-Hua Zhou. Partial multi-view clustering. In *Proceedings of the AAAI Conference on Artificial Intelligence*, pages 1968–1974, 2014.
- [13] Yijie Lin, Yuanbiao Gou, Zitao Liu, Boyun Li, Jiancheng Lv, and Xi Peng. COMPLETER: Incomplete multi-view clustering via contrastive prediction. In *Proceedings of the IEEE/CVF Conference on Computer Vision and Pattern Recognition (CVPR)*, pages 11174–11183, 2021.
- [14] Yijie Lin, Yuanbiao Gou, Xiaotian Liu, Jinfeng Bai, Jiancheng Lv, and Xi Peng. Dual contrastive prediction for incomplete multi-view representation learning. *IEEE Transactions on Pattern Analysis and Machine Intelligence*, 45(4):4447–4461, 2023.
- [15] Ruimeng Liu, Xin Zou, Chang Tang, Xiao Zheng, Xingchen Hu, Kun Sun, and Xinwang Liu. SparseMVC: Probing cross-view sparsity variations for multi-view clustering. In *The Thirtieth Annual Conference on Neural Information Processing Systems (NeurIPS)*, 2026. URL <https://openreview.net/forum?id=cvJvk6oYfC>.
- [16] Xinwang Liu, Miaomiao Li, Lei Wang, Yong Dou, Jianping Yin, and En Zhu. Multiple kernel k-means with incomplete kernels. In *Proceedings of the AAAI Conference on Artificial Intelligence*, pages 2259–2265, 2017.

- [17] Mengmeng Ma, Jian Ren, Long Zhao, Davide Testuggine, and Xi Peng. Are multimodal transformers robust to missing modality? In *Proceedings of the IEEE/CVF Conference on Computer Vision and Pattern Recognition (CVPR)*, pages 18177–18186, 2022.
- [18] Weixiang Shao, Lifang He, and Philip S. Yu. Multiple incomplete views clustering via weighted nonnegative matrix factorization with $l_{2,1}$ regularization. In *ECML/PKDD*, 2015.
- [19] Huayi Tang and Yong Liu. Deep safe incomplete multi-view clustering: Theorem and algorithm. In *Proceedings of the 39th International Conference on Machine Learning (ICML)*, Proceedings of Machine Learning Research, pages 21090–21110, 2022.
- [20] Huayi Tang and Yong Liu. Deep safe multi-view clustering: Reducing the risk of clustering performance degradation caused by view increase. In *Proceedings of the IEEE/CVF Conference on Computer Vision and Pattern Recognition (CVPR)*, pages 202–211, 2022.
- [21] Ashish Vaswani, Noam Shazeer, Niki Parmar, Jakob Uszkoreit, Llion Jones, Aidan N Gomez, Łukasz Kaiser, and Illia Polosukhin. Attention is all you need. In *Advances in Neural Information Processing Systems (NeurIPS)*, pages 6000–6010, 2017.
- [22] Hao Wang, Linlin Zong, Bing Liu, Yan Yang, and Wei Zhou. Spectral perturbation meets incomplete multi-view data. In *Proceedings of the Twenty-Eighth International Joint Conference on Artificial Intelligence (IJCAI)*, pages 3677–3683, 2019.
- [23] Qianqian Wang, Zhengming Ding, Zhiqiang Tao, Quanxue Gao, and Yun Fu. Generative partial multi-view clustering with adaptive fusion and cycle consistency. *IEEE Transactions on Image Processing*, 30:1771–1783, 2021. doi: 10.1109/TIP.2020.3048626.
- [24] Ziyu Wang, Yiming Du, Rui Ning, and Lusi Li. Energy-based deep incomplete multi-view clustering. In *Proceedings of the 33rd ACM International Conference on Multimedia (MM '25)*, pages 1686–1694. ACM, 2025.
- [25] Jie Wen, Zheng Zhang, Yong Xu, Bob Zhang, Lunke Fei, and Hong Liu. Unified embedding alignment with missing views inferring for incomplete multi-view clustering. In *Proceedings of the AAAI Conference on Artificial Intelligence*, 2019. doi: 10.1609/aaai.v33i01.33015393.
- [26] Jie Wen, Zheng Zhang, Yong Xu, Bob Zhang, Lunke Fei, and Guo-Sen Xie. CDIMC-net: Cognitive deep incomplete multi-view clustering network. In *Proceedings of the Twenty-Ninth International Joint Conference on Artificial Intelligence (IJCAI)*, pages 3230–3236, 2020. doi: 10.24963/ijcai.2020/447.
- [27] Jie Wen, Zheng Zhang, Lunke Fei, Bob Zhang, Yong Xu, Zhao Zhang, and Jinxing Li. A survey on incomplete multiview clustering. *IEEE Transactions on Systems, Man, and Cybernetics: Systems*, 53(2):1136–1149, 2022.
- [28] Benyu Wu, Wei Du, Jun Wang, and Guoxian Yu. Imputation-free incomplete multi-view clustering via knowledge distillation. In *Proceedings of the Thirty-Fourth International Joint Conference on Artificial Intelligence (IJCAI)*, pages 6570–6578, 2025.
- [29] Jie Xu, Huayi Tang, Yazhou Ren, Liang Peng, Xiaofeng Zhu, and Lifang He. Multi-level feature learning for contrastive multi-view clustering. In *Proceedings of the IEEE/CVF Conference on Computer Vision and Pattern Recognition (CVPR)*, pages 16030–16039, 2022.
- [30] Jie Xu, Chao Li, Liang Peng, Yazhou Ren, Xiaoshuang Shi, Heng Tao Shen, and Xiaofeng Zhu. Adaptive feature projection with distribution alignment for deep incomplete multi-view clustering. *IEEE Transactions on Image Processing*, 32:1354–1366, 2023.
- [31] Mouxing Yang, Yunfan Li, Zhenyu Huang, Zitao Liu, Peng Hu, and Xi Peng. Partially view-aligned representation learning with noise-robust contrastive loss. In *Proceedings of the IEEE/CVF Conference on Computer Vision and Pattern Recognition (CVPR)*, pages 1134–1143, 2021.
- [32] Mouxing Yang, Yunfan Li, Peng Hu, Jinfeng Bai, Jiancheng Lv, and Xi Peng. Robust multi-view clustering with incomplete information. *IEEE Transactions on Pattern Analysis and Machine Intelligence*, 45(1):1055–1069, 2023. doi: 10.1109/TPAMI.2022.3155499.

- [33] Manzil Zaheer, Satwik Kottur, Siamak Ravanbakhsh, Barnabás Póczos, Russ R Salakhutdinov, and Alexander J Smola. Deep sets. In *Advances in Neural Information Processing Systems (NeurIPS)*, pages 3391–3401, 2017.
- [34] Yuanyang Zhang, Yijie Lin, Weiqing Yan, Li Yao, Xinhang Wan, Guangyuan Li, Chao Zhang, Guanzhou Ke, and Jie Xu. Incomplete multi-view clustering via diffusion contrastive generation. In *Proceedings of the AAAI Conference on Artificial Intelligence*, volume 39, pages 22650–22658, 2025.
- [35] Handong Zhao, Hongfu Liu, and Yun Fu. Incomplete multi-modal visual data grouping. In *Proceedings of the Twenty-Fifth International Joint Conference on Artificial Intelligence (IJ-CAI)*, pages 2392–2398, 2016.

NeurIPS Paper Checklist

1. Claims

Question: Do the main claims made in the abstract and introduction accurately reflect the paper’s contributions and scope?

Answer: [Yes]

Justification: The abstract and Section 1 outline the contributions: formalizing incompleteness divergence (\hat{r}, p_c), proving the \mathcal{F}_{rec} trainability bound (Theorem 4.2), the CRAFT architecture, and empirical validation on seven benchmarks.

Guidelines:

- The answer [N/A] means that the abstract and introduction do not include the claims made in the paper.
- The abstract and/or introduction should clearly state the claims made, including the contributions made in the paper and important assumptions and limitations. A [No] or [N/A] answer to this question will not be perceived well by the reviewers.
- The claims made should match theoretical and experimental results, and reflect how much the results can be expected to generalize to other settings.
- It is fine to include aspirational goals as motivation as long as it is clear that these goals are not attained by the paper.

2. Limitations

Question: Does the paper discuss the limitations of the work performed by the authors?

Answer: [Yes]

Justification: The Conclusion (Section 7) explicitly notes that CRAFT addresses only the cross-view reconstruction loss family in unsupervised IMVC and points to supervised or distributional multi-view extensions as future work.

Guidelines:

- The answer [N/A] means that the paper has no limitation while the answer [No] means that the paper has limitations, but those are not discussed in the paper.
- The authors are encouraged to create a separate “Limitations” section in their paper.
- The paper should point out any strong assumptions and how robust the results are to violations of these assumptions (e.g., independence assumptions, noiseless settings, model well-specification, asymptotic approximations only holding locally). The authors should reflect on how these assumptions might be violated in practice and what the implications would be.
- The authors should reflect on the scope of the claims made, e.g., if the approach was only tested on a few datasets or with a few runs. In general, empirical results often depend on implicit assumptions, which should be articulated.
- The authors should reflect on the factors that influence the performance of the approach. For example, a facial recognition algorithm may perform poorly when image resolution is low or images are taken in low lighting. Or a speech-to-text system might not be used reliably to provide closed captions for online lectures because it fails to handle technical jargon.

- The authors should discuss the computational efficiency of the proposed algorithms and how they scale with dataset size.
- If applicable, the authors should discuss possible limitations of their approach to address problems of privacy and fairness.
- While the authors might fear that complete honesty about limitations might be used by reviewers as grounds for rejection, a worse outcome might be that reviewers discover limitations that aren't acknowledged in the paper. The authors should use their best judgment and recognize that individual actions in favor of transparency play an important role in developing norms that preserve the integrity of the community. Reviewers will be specifically instructed to not penalize honesty concerning limitations.

3. Theory assumptions and proofs

Question: For each theoretical result, does the paper provide the full set of assumptions and a complete (and correct) proof?

Answer: [Yes]

Justification: Theorem 4.1, Proposition 4.1, Theorem 4.2, and Corollary 4.1 are stated with explicit assumptions in Section 4; full proofs appear in Appendix B.

Guidelines:

- The answer [N/A] means that the paper does not include theoretical results.
- All the theorems, formulas, and proofs in the paper should be numbered and cross-referenced.
- All assumptions should be clearly stated or referenced in the statement of any theorems.
- The proofs can either appear in the main paper or the supplemental material, but if they appear in the supplemental material, the authors are encouraged to provide a short proof sketch to provide intuition.
- Inversely, any informal proof provided in the core of the paper should be complemented by formal proofs provided in appendix or supplemental material.
- Theorems and Lemmas that the proof relies upon should be properly referenced.

4. Experimental result reproducibility

Question: Does the paper fully disclose all the information needed to reproduce the main experimental results of the paper to the extent that it affects the main claims and/or conclusions of the paper (regardless of whether the code and data are provided or not)?

Answer: [Yes]

Justification: Architecture details are in Section 5, the training algorithm is given as Algorithm 1 in Appendix A.5, per-dataset hyperparameters in Appendix A.2, and the seed protocol and hardware in Appendix A.1.

Guidelines:

- The answer [N/A] means that the paper does not include experiments.
- If the paper includes experiments, a [No] answer to this question will not be perceived well by the reviewers: Making the paper reproducible is important, regardless of whether the code and data are provided or not.
- If the contribution is a dataset and/or model, the authors should describe the steps taken to make their results reproducible or verifiable.
- Depending on the contribution, reproducibility can be accomplished in various ways. For example, if the contribution is a novel architecture, describing the architecture fully might suffice, or if the contribution is a specific model and empirical evaluation, it may be necessary to either make it possible for others to replicate the model with the same dataset, or provide access to the model. In general, releasing code and data is often one good way to accomplish this, but reproducibility can also be provided via detailed instructions for how to replicate the results, access to a hosted model (e.g., in the case of a large language model), releasing of a model checkpoint, or other means that are appropriate to the research performed.

- While NeurIPS does not require releasing code, the conference does require all submissions to provide some reasonable avenue for reproducibility, which may depend on the nature of the contribution. For example
 - (a) If the contribution is primarily a new algorithm, the paper should make it clear how to reproduce that algorithm.
 - (b) If the contribution is primarily a new model architecture, the paper should describe the architecture clearly and fully.
 - (c) If the contribution is a new model (e.g., a large language model), then there should either be a way to access this model for reproducing the results or a way to reproduce the model (e.g., with an open-source dataset or instructions for how to construct the dataset).
 - (d) We recognize that reproducibility may be tricky in some cases, in which case authors are welcome to describe the particular way they provide for reproducibility. In the case of closed-source models, it may be that access to the model is limited in some way (e.g., to registered users), but it should be possible for other researchers to have some path to reproducing or verifying the results.

5. Open access to data and code

Question: Does the paper provide open access to the data and code, with sufficient instructions to faithfully reproduce the main experimental results, as described in supplemental material?

Answer: [Yes]

Justification: Two anonymous links are provided in the supplementary material: the CRAFT implementation (<https://anonymous.4open.science/r/CRAFT-BF80/>) and a standalone imvc-audit evaluation toolkit (<https://anonymous.4open.science/r/imvc-audit-8263/>). All seven benchmarks (CUB, MultiFashion, HandWritten, UCI-Digit, Out-Scene, Caltech, YTF-31) are publicly available.

Guidelines:

- The answer [N/A] means that paper does not include experiments requiring code.
- Please see the NeurIPS code and data submission guidelines (<https://neurips.cc/public/guides/CodeSubmissionPolicy>) for more details.
- While we encourage the release of code and data, we understand that this might not be possible, so [No] is an acceptable answer. Papers cannot be rejected simply for not including code, unless this is central to the contribution (e.g., for a new open-source benchmark).
- The instructions should contain the exact command and environment needed to run to reproduce the results. See the NeurIPS code and data submission guidelines (<https://neurips.cc/public/guides/CodeSubmissionPolicy>) for more details.
- The authors should provide instructions on data access and preparation, including how to access the raw data, preprocessed data, intermediate data, and generated data, etc.
- The authors should provide scripts to reproduce all experimental results for the new proposed method and baselines. If only a subset of experiments are reproducible, they should state which ones are omitted from the script and why.
- At submission time, to preserve anonymity, the authors should release anonymized versions (if applicable).
- Providing as much information as possible in supplemental material (appended to the paper) is recommended, but including URLs to data and code is permitted.

6. Experimental setting/details

Question: Does the paper specify all the training and test details (e.g., data splits, hyperparameters, how they were chosen, type of optimizer) necessary to understand the results?

Answer: [Yes]

Justification: Section 6.1 describes the baselines, protocol grid, and metrics; Appendix A.2 provides per-dataset hyperparameters and the training schedule.

Guidelines:

- The answer [N/A] means that the paper does not include experiments.
- The experimental setting should be presented in the core of the paper to a level of detail that is necessary to appreciate the results and make sense of them.
- The full details can be provided either with the code, in appendix, or as supplemental material.

7. Experiment statistical significance

Question: Does the paper report error bars suitably and correctly defined or other appropriate information about the statistical significance of the experiments?

Answer: [Yes]

Justification: All main-text experiments report 5-seed mean \pm standard deviation (seeds 42–46). YTF-31 is single-seed due to dataset scale ($n \approx 100k$); this is explicitly stated in Appendix A.1.

Guidelines:

- The answer [N/A] means that the paper does not include experiments.
- The authors should answer [Yes] if the results are accompanied by error bars, confidence intervals, or statistical significance tests, at least for the experiments that support the main claims of the paper.
- The factors of variability that the error bars are capturing should be clearly stated (for example, train/test split, initialization, random drawing of some parameter, or overall run with given experimental conditions).
- The method for calculating the error bars should be explained (closed form formula, call to a library function, bootstrap, etc.)
- The assumptions made should be given (e.g., Normally distributed errors).
- It should be clear whether the error bar is the standard deviation or the standard error of the mean.
- It is OK to report 1-sigma error bars, but one should state it. The authors should preferably report a 2-sigma error bar than state that they have a 96% CI, if the hypothesis of Normality of errors is not verified.
- For asymmetric distributions, the authors should be careful not to show in tables or figures symmetric error bars that would yield results that are out of range (e.g., negative error rates).
- If error bars are reported in tables or plots, the authors should explain in the text how they were calculated and reference the corresponding figures or tables in the text.

8. Experiments compute resources

Question: For each experiment, does the paper provide sufficient information on the computer resources (type of compute workers, memory, time of execution) needed to reproduce the experiments?

Answer: [Yes]

Justification: Appendix A.1 specifies the hardware (single NVIDIA RTX 3090, 24GB VRAM, PyTorch 2.1, CUDA 12.1); per-run wall-clock times are reported in Appendix D.8.

Guidelines:

- The answer [N/A] means that the paper does not include experiments.
- The paper should indicate the type of compute workers CPU or GPU, internal cluster, or cloud provider, including relevant memory and storage.
- The paper should provide the amount of compute required for each of the individual experimental runs as well as estimate the total compute.
- The paper should disclose whether the full research project required more compute than the experiments reported in the paper (e.g., preliminary or failed experiments that didn't make it into the paper).

9. Code of ethics

Question: Does the research conducted in the paper conform, in every respect, with the NeurIPS Code of Ethics <https://neurips.cc/public/EthicsGuidelines?>

Answer: [Yes]

Justification: This research adheres to the NeurIPS Code of Ethics. The work does not involve human subjects, scraped data, or privacy-sensitive material.

Guidelines:

- The answer [N/A] means that the authors have not reviewed the NeurIPS Code of Ethics.
- If the authors answer [No], they should explain the special circumstances that require a deviation from the Code of Ethics.
- The authors should make sure to preserve anonymity (e.g., if there is a special consideration due to laws or regulations in their jurisdiction).

10. Broader impacts

Question: Does the paper discuss both potential positive societal impacts and negative societal impacts of the work performed?

Answer: [N/A]

Justification: Multi-view clustering is foundational unsupervised learning research with no easily predictable direct path to negative societal impacts.

Guidelines:

- The answer [N/A] means that there is no societal impact of the work performed.
- If the authors answer [N/A] or [No], they should explain why their work has no societal impact or why the paper does not address societal impact.
- Examples of negative societal impacts include potential malicious or unintended uses (e.g., disinformation, generating fake profiles, surveillance), fairness considerations (e.g., deployment of technologies that could make decisions that unfairly impact specific groups), privacy considerations, and security considerations.
- The conference expects that many papers will be foundational research and not tied to particular applications, let alone deployments. However, if there is a direct path to any negative applications, the authors should point it out. For example, it is legitimate to point out that an improvement in the quality of generative models could be used to generate Deepfakes for disinformation. On the other hand, it is not needed to point out that a generic algorithm for optimizing neural networks could enable people to train models that generate Deepfakes faster.
- The authors should consider possible harms that could arise when the technology is being used as intended and functioning correctly, harms that could arise when the technology is being used as intended but gives incorrect results, and harms following from (intentional or unintentional) misuse of the technology.
- If there are negative societal impacts, the authors could also discuss possible mitigation strategies (e.g., gated release of models, providing defenses in addition to attacks, mechanisms for monitoring misuse, mechanisms to monitor how a system learns from feedback over time, improving the efficiency and accessibility of ML).

11. Safeguards

Question: Does the paper describe safeguards that have been put in place for responsible release of data or models that have a high risk for misuse (e.g., pre-trained language models, image generators, or scraped datasets)?

Answer: [N/A]

Justification: This work does not release high-risk models or datasets requiring safeguards; CRAFT is a clustering model trained on publicly available benchmarks.

Guidelines:

- The answer [N/A] means that the paper poses no such risks.
- Released models that have a high risk for misuse or dual-use should be released with necessary safeguards to allow for controlled use of the model, for example by requiring that users adhere to usage guidelines or restrictions to access the model or implementing safety filters.

- Datasets that have been scraped from the Internet could pose safety risks. The authors should describe how they avoided releasing unsafe images.
- We recognize that providing effective safeguards is challenging, and many papers do not require this, but we encourage authors to take this into account and make a best faith effort.

12. Licenses for existing assets

Question: Are the creators or original owners of assets (e.g., code, data, models), used in the paper, properly credited and are the license and terms of use explicitly mentioned and properly respected?

Answer: [Yes]

Justification: All seven benchmarks are publicly available datasets standard in the IMVC literature. CUB and HandWritten (mfeat) are shipped pre-processed in the anonymous CRAFT repository ([data/](#)); per-dataset download links and preprocessing notes for the remaining five benchmarks (MultiFashion, UCI-Digit, Out-Scene, Caltech, YTF-31) are provided in the repository README. Each baseline implementation cites the original method paper (COMPLETER, DCP, DCG, ProImp, HSACC, Energy-DIMC, DVIMC).

Guidelines:

- The answer [N/A] means that the paper does not use existing assets.
- The authors should cite the original paper that produced the code package or dataset.
- The authors should state which version of the asset is used and, if possible, include a URL.
- The name of the license (e.g., CC-BY 4.0) should be included for each asset.
- For scraped data from a particular source (e.g., website), the copyright and terms of service of that source should be provided.
- If assets are released, the license, copyright information, and terms of use in the package should be provided. For popular datasets, [paperswithcode.com/datasets](#) has curated licenses for some datasets. Their licensing guide can help determine the license of a dataset.
- For existing datasets that are re-packaged, both the original license and the license of the derived asset (if it has changed) should be provided.
- If this information is not available online, the authors are encouraged to reach out to the asset's creators.

13. New assets

Question: Are new assets introduced in the paper well documented and is the documentation provided alongside the assets?

Answer: [Yes]

Justification: The anonymous supplementary material includes two repositories: (1) the CRAFT implementation, and (2) the `imvc-audit` standalone evaluation toolkit (Python package with closed-form \hat{r} and p_c formulas, mask sampling utilities, and a CLI) for cross-protocol IMVC audit.

Guidelines:

- The answer [N/A] means that the paper does not release new assets.
- Researchers should communicate the details of the dataset/code/model as part of their submissions via structured templates. This includes details about training, license, limitations, etc.
- The paper should discuss whether and how consent was obtained from people whose asset is used.
- At submission time, remember to anonymize your assets (if applicable). You can either create an anonymized URL or include an anonymized zip file.

14. Crowdsourcing and research with human subjects

Question: For crowdsourcing experiments and research with human subjects, does the paper include the full text of instructions given to participants and screenshots, if applicable, as well as details about compensation (if any)?

Answer: [N/A]

Justification: This paper does not involve crowdsourcing or research with human subjects.

Guidelines:

- The answer [N/A] means that the paper does not involve crowdsourcing nor research with human subjects.
- Including this information in the supplemental material is fine, but if the main contribution of the paper involves human subjects, then as much detail as possible should be included in the main paper.
- According to the NeurIPS Code of Ethics, workers involved in data collection, curation, or other labor should be paid at least the minimum wage in the country of the data collector.

15. Institutional review board (IRB) approvals or equivalent for research with human subjects

Question: Does the paper describe potential risks incurred by study participants, whether such risks were disclosed to the subjects, and whether Institutional Review Board (IRB) approvals (or an equivalent approval/review based on the requirements of your country or institution) were obtained?

Answer: [N/A]

Justification: This research does not involve human subjects, so IRB approval is not required.

Guidelines:

- The answer [N/A] means that the paper does not involve crowdsourcing nor research with human subjects.
- Depending on the country in which research is conducted, IRB approval (or equivalent) may be required for any human subjects research. If you obtained IRB approval, you should clearly state this in the paper.
- We recognize that the procedures for this may vary significantly between institutions and locations, and we expect authors to adhere to the NeurIPS Code of Ethics and the guidelines for their institution.
- For initial submissions, do not include any information that would break anonymity (if applicable), such as the institution conducting the review.

16. Declaration of LLM usage

Question: Does the paper describe the usage of LLMs if it is an important, original, or non-standard component of the core methods in this research? Note that if the LLM is used only for writing, editing, or formatting purposes and does *not* impact the core methodology, scientific rigor, or originality of the research, declaration is not required.

Answer: [N/A]

Justification: The core method development does not involve LLMs as any important, original, or non-standard component.

Guidelines:

- The answer [N/A] means that the core method development in this research does not involve LLMs as any important, original, or non-standard components.
- Please refer to our LLM policy in the NeurIPS handbook for what should or should not be described.

A Experimental Details

A.1 Datasets and Hardware

Table 3 summarizes the seven benchmarks used in this work.

Table 3: Dataset overview.

Dataset	N	V	K	d_{total}
CUB	600	2	10	1,324
MultiFashion	10,000	3	10	1,176
UCI-digit	2,000	3	10	356
Out-Scene	2,688	4	8	1,248
HandWritten	2,000	6	10	649
Caltech	2,386	6	20	3,766
YTF-31	101,499	5	31	2,125

All experiments are conducted on a single NVIDIA RTX 3090 GPU (24 GB VRAM) with PyTorch 2.1 and CUDA 12.1. All timing measurements are wall-clock times on this hardware. Reported numbers are mean \pm std across 5 random seeds (seeds 42–46), except YTF-31 where dataset scale limits us to a single run (seed 42).

A.2 CRAFT Hyperparameters

Table 4 lists the full per-dataset configuration. All datasets share the same architecture (single-layer Transformer with 4 heads, 2-layer MLP encoder and symmetric decoder) and optimizer (AdamW, weight decay 10^{-4} , batch size 256). Each configuration is tuned once on complete data; the resulting checkpoint handles all missing patterns and protocols without further adjustment.

Table 4: Per-dataset hyperparameter configuration. “Default” denotes the shared configuration used by HW and UCI without modification.

Parameter	Default	CUB	MF	OS	Cal	YTF
encoder_type	deep	deep	shallow	deep	shallow	deep
encoder_hidden	512	512	1024	512	512	1024
embed_dim d	256	128	256	256	256	512
τ	0.5	0.5	0.03	0.1	0.5	0.5
λ_{ent}	5.0	5.0	0.5	5.0	0.1	0.1
dropout	0.1	0.1	0.03	0.1	0.1	0.1
noise_std	0.1	0.1	0.03	0.1	0.1	0.1
Stage 1 epochs	100	100	200	100	100	100
Stage 2 epochs	100	100	200	100	100	80
Stage 1 lr	5e-4	5e-4	5e-4	5e-4	5e-4	5e-4
Stage 2 lr	1e-5	1e-5	5e-5	1e-4	2e-4	1e-6

CUB uses $d=128$ because the small sample size ($n=600$) leads to overfitting at $d=256$. Caltech and MultiFashion use shallow encoders ($d_v \rightarrow d$) because their high-dimensional views cause training instability with deeper encoders. YTF-31 uses a wider architecture ($d=512$, hidden=1024) to accommodate its larger scale and higher class count ($K=31$). MFT uses 100 epochs at 10^{-5} for HW and Out-Scene; MultiFashion MFT uses 300 epochs at 10^{-5} , resuming from the Stage 2 checkpoint.

A.3 Baseline Reproduction

This section consolidates reproduction details, protocol inferences, and failure analyses for all baseline methods.

A.3.1 DCG Configuration

The official DCG repository contains no multi-view configuration beyond two views. We extend the released two-view script to accept all views, retaining all other hyperparameters at their official values.

A.3.2 View Selection Audit

On HandWritten ($V=6$, $n=2,000$), the official DCG and ProImp codebases load only 2 of the 6 views: DCG selects views 2 and 3 (76d and 64d), discarding 78% of the total feature dimensions—a choice not documented in the corresponding paper. ProImp’s encoder pair is hardcoded to 2 views by construction. The DCG numbers reported in this paper instead use our 6-view extension (Appendix A.3.1), which accesses all six views while retaining DCG’s other hyperparameters at their official values. ProImp and APADC are architecturally limited to two views and are not extended in this work.

A.3.3 DCP and DSIMVC Implementation

DCP. DCP shares its masking utility with COMPLETER (same research group and codebase); its behavior matches Protocol 2 (§3.2).

DSIMVC. Generates masks by drawing a per-sample Bernoulli trial at rate r , then deleting one randomly chosen view for each selected sample. A post-processing step ensures at least one view per sample. This is equivalent to Protocol 1 with Bernoulli rather than fixed-count sampling; the difference is negligible for large n .

Evaluation randomness. In DCG, the outer-loop variable intended to vary across repeated runs is not connected to the random seed; a fixed seed produces the same mask and training trajectory in every iteration, reducing the effective number of independent trials to one. In ProImp, the mask seed varies but the training seed is fixed. In both cases the reported variance understates the true run-to-run variability.

A.3.4 BURG Protocol Inference

BURG [9] does not specify its masking procedure. We classify it as Protocol 2 by convention: BURG benchmarks against COMPLETER, DCP, and APADC at identical nominal rates ($MR \in \{0.1, 0.3, 0.5, 0.7\}$) without discussing protocol differences, and our audit (§C.4) verified by code inspection that these three baselines realize Protocol 2 via a shared entry-wise Bernoulli with protected-view masking codebase. This suggests BURG inherits the same masking convention, though the classification is not directly verifiable from the paper alone.

A.3.5 DVIMC Failure on Multi-View Datasets

DVIMC’s K-Means initialization step assumes a fixed input dimension across all samples. When the protocol produces samples with $|O_i| = 0$, this assumption is violated and initialization fails outright—a structural C2 violation. We attribute DVIMC’s `ValueError` crashes on MultiFashion at $r=0.7$ (Protocol 4), CUB at $r \geq 0.5$ (Protocol 4), and HandWritten under Protocols 3–4 at $r=0.7$ to this mechanism. The K-Means crash is the only DVIMC failure mode we attribute to C2 violation.

Beyond the C2 violation: heterogeneous multi-view weakness. Single-seed evaluation of DVIMC across all 16 (protocol, rate) configurations (seed 42, official implementation [2]) on CUB ($V=2$) and HandWritten ($V=6$) reveals failure modes beyond the K-Means crash. On CUB, accuracy stays in the 20–28% range across all 16 configurations (random baseline 10% at $K=10$); on HandWritten, accuracy swings non-monotonically across configurations from 17.55% (Protocol 3 at $r=0.3$) to 91.65% (Protocol 2 at $r=0.1$). These patterns are not predicted by C2 violation alone. They reflect implementation-level factors of DVIMC’s official codebase: hyperparameters tuned for the four datasets in the original paper rather than these benchmarks; a coherence loss enforcing posterior agreement across views, which destabilizes when views are heterogeneous; product-of-experts aggregation that is sensitive to view-quality imbalance; and naive view-latent averaging during K-Means initialization that dilutes informative views with weaker ones. Under HandWritten’s six-view feature scales (dimensions $\{240, 216, 76, 64, 47, 6\}$), these factors compound. The instability is therefore better characterized as “DVIMC’s reference implementation does not generalize to heterogeneous multi-view data with high view counts” rather than as an architectural-class statement; the C2-violation failure mode (K-Means crash at $|O_i| = 0$) is the architectural finding on which this paper relies, and it remains the only DVIMC observation we treat as evidence for C2 necessity.

Under the identical 16 configurations, the canonical CRAFT checkpoint produces non-trivial accuracy on every condition with no crashes (Table 8).

A.4 Tuning of Collapsed Baselines

To confirm that the trainability collapse documented in §6.2 is structural rather than a tuning artifact, we tuned DCG ($\text{lr} \in \{1\text{e-}3, 5\text{e-}4, 1\text{e-}4\}$, $\tau \in \{0.5, 0.3, 0.1\}$) and DCP ($\text{lr} \in \{1\text{e-}3, 5\text{e-}4, 1\text{e-}4\}$) under Protocol 4 on CUB ($V=2$, $r=0.5$, $p_c=0$). No DCG configuration exceeded 20.17% ACC and no DCP configuration exceeded 36.83% (random baseline 10%). The collapse is therefore driven by the structural absence of complete samples ($p_c=0$), not by suboptimal hyperparameters.

A.5 Training Algorithm

Algorithm 1 CRAFT training (complete-data, two-stage)

Require: complete samples $\{x^{(i)}\}_{i=1}^n$; encoder θ , head ϕ ; epochs E_1, E_2 ; coefficients $\lambda_{\text{repr}}, \beta, \gamma$

- 1: **for** $e = 1$ **to** E_1 {Stage 1: representation learning} **do**
- 2: Sample batch; compute $z_v = E_v(x_v)$ for $v = 1:V$
- 3: $h \leftarrow \text{Transformer}([\text{CLS}], z_1, \dots, z_V)$ (no mask)
- 4: Update θ on $\mathcal{L}_{\text{stage1}}$ (Eq. 2)
- 5: **end for**
- 6: **for** $e = 1$ **to** E_2 {Stage 2: cluster fine-tuning} **do**
- 7: Sample batch; optionally apply MFT random view mask
- 8: $h \leftarrow \text{Transformer}([\text{CLS}], z_1, \dots, z_V)$; mask
- 9: Update θ, ϕ on $\mathcal{L}_{\text{stage2}}$ (Eq. 3)
- 10: **end for**
- 11: **Inference (any protocol):** forward pass with key-padding mask set from O_i .

A.6 Loss Component Definitions

The Stage 1 and Stage 2 losses (Eqs. 2–3) decompose into the following per-sample terms.

$\mathcal{L}_{\text{recon}}$ (**per-view reconstruction**). $\mathcal{L}_{\text{recon}} = \frac{1}{n} \sum_{i=1}^n \sum_{v=1}^V \|D_v(h^{(i)}) - x_v^{(i)}\|^2$, where D_v is a view-specific decoder MLP.

$\mathcal{L}_{\text{repr}}$ (**cross-view consistency**). $\mathcal{L}_{\text{repr}} = -\frac{1}{nV(V-1)} \sum_i \sum_{v \neq v'} \cos(P_\phi(z_v^{(i)}), \text{sg}(z_{v'}^{(i)}))$, with predictor MLP P_ϕ and stop-gradient $\text{sg}(\cdot)$ [3].

$\mathcal{L}_{\text{cluster}}$ (**self-labeled cross-entropy**). $\mathcal{L}_{\text{cluster}} = -\frac{1}{n} \sum_{i=1}^n \log p_{\hat{y}^{(i)}}(h^{(i)})$, $p_k(h) = \text{softmax}_k(\tau \cos(h, c_k))$, where $\hat{y}^{(i)} = \arg \max_k p_k(h^{(i)})$ are pseudo-labels refreshed each epoch and $\{c_k\}_{k=1}^K$ are unit-norm prototypes.

\mathcal{L}_{ent} (**anti-collapse entropy**). $\mathcal{L}_{\text{ent}} = \sum_{k=1}^K \bar{p}_k \log \bar{p}_k$, $\bar{p}_k = \frac{1}{n} \sum_{i=1}^n p_k(h^{(i)})$. Minimizing this term pushes the batch-averaged prediction toward uniform over K clusters, preventing degenerate single-cluster solutions.

\mathcal{L}_{KL} (**MFT consistency**). For two MFT-sampled view-subsets $S_1, S_2 \subseteq O_i$ of sample i (§5.3), $\mathcal{L}_{\text{KL}} = \frac{1}{n} \sum_{i=1}^n \text{KL}(p(\cdot | h_{S_1}^{(i)}) \| p(\cdot | h_{S_2}^{(i)}))$, with $\gamma = 0$ when MFT is disabled.

A.7 PyTorch Inference Snippet

The following snippet illustrates CRAFT’s inference-time handling of missing views. No special module is required; the standard PyTorch MultiheadAttention accepts a key-padding mask directly.

```
# tokens: [batch, 1+V, d] (CLS + V view embeddings)
# missing: [batch, V] bool (True = view absent)
pad = torch.zeros(B, 1+V, dtype=torch.bool) # CLS never masked
pad[:, 1:] = missing
h = transformer_encoder(tokens, src_key_padding_mask=pad)
h_cls = h[:, 0] # fused representation
pred = cosine_softmax(h_cls, centroids, tau)
```

B Proofs

B.1 Proof of Proposition 4.1 (Trainability Bound for \mathcal{F}_{rec})

Proof of Proposition 4.1. Setup. Consider the recovery loss $\mathcal{L}_{rec}(\theta, \phi)$, which is computed exclusively over cross-view pairs from complete samples. In a mini-batch of size B drawn uniformly at random, $B_c \sim \text{Binomial}(B, p_c)$ complete samples are present. The stochastic gradient estimator for the recovery branch is

$$g_t = \begin{cases} \frac{1}{B_c} \sum_{i \in C_{\text{batch}}} \nabla \mathcal{L}_{rec}^{(i)}(\theta_t), & B_c \geq 1, \\ \mathbf{0}, & B_c = 0. \end{cases}$$

We assume \mathcal{L}_{rec} is L -smooth, each per-sample gradient has bounded variance σ^2 , and mini-batches are sampled i.i.d. uniformly.

Step 1: Decomposition into active and inactive steps. Define $\beta_t = \mathbb{1}[B_c^{(t)} \geq 1]$, an i.i.d. Bernoulli variable with success probability $\beta \equiv 1 - (1 - p_c)^B$.² When $\beta_t = 0$, the gradient is zero and $\theta_{t+1} = \theta_t$; the parameter is unchanged. The sequence of parameter values at *active* steps follows exactly the trajectory of standard SGD applied to \mathcal{L}_{rec} with effective batch size B_c drawn from $(B_c | B_c \geq 1)$.

Step 2: Effective batch size at active steps. The conditional expectation of the batch size at active steps is

$$b_{\text{eff}} = \mathbb{E}[B_c | B_c \geq 1] = \frac{Bp_c}{1 - (1 - p_c)^B} = \frac{Bp_c}{\beta}.$$

When $Bp_c \gg 1$: $\beta \approx 1$ and $b_{\text{eff}} \approx Bp_c$. When $Bp_c \ll 1$: $\beta \approx Bp_c$ and $b_{\text{eff}} \approx 1$ —the rare active batches contain almost surely a single complete sample.

By Jensen’s inequality, the per-step gradient variance satisfies $\mathbb{E}[\sigma^2/B_c | B_c \geq 1] \geq \sigma^2/b_{\text{eff}}$.

Step 3: Convergence rate. Applying the standard non-convex SGD convergence result to the $T_{\text{active}} \approx \beta T$ active steps with per-step variance at least σ^2/b_{eff} , the ε -stationarity requirement $\min_t \mathbb{E}[\|\nabla \mathcal{L}_{rec}\|^2] \leq \varepsilon$ demands:

$$T_{\text{active}} \geq \Omega\left(\frac{L\Delta\sigma^2}{b_{\text{eff}} \cdot \varepsilon^2}\right) = \Omega\left(\frac{L\Delta\sigma^2\beta}{Bp_c \cdot \varepsilon^2}\right).$$

Since $T = T_{\text{active}}/\beta$, the total iteration count is

$$T \geq \Omega\left(\frac{L\Delta\sigma^2}{Bp_c \cdot \varepsilon^2}\right) = \frac{1}{p_c} \Omega\left(\frac{L\Delta\sigma^2}{B \cdot \varepsilon^2}\right).$$

The β factors cancel: the active-step probability reduces the number of useful steps, but the reduced batch size at active steps increases per-step variance by the same factor. The net effect is a clean $1/p_c$ slowdown relative to the standard rate T_0 .

² β in this proof denotes the active-batch fraction; it is local to Appendix B.1 and distinct from the entropy regularizer coefficient β of §5.2.

Step 4: Characteristic scale and transition sharpness. The fraction of batches receiving any recovery gradient is $\beta = 1 - (1 - p_c)^B$. This function transitions from $\beta \approx 0$ to $\beta \approx 1$ over the interval $p_c \in [p_{lo}, p_{hi}]$ where $p_{lo} = 1 - 0.9^{1/B}$ (10% active batches) and $p_{hi} = 1 - 0.1^{1/B}$ (90% active batches). For $B = 256$: $p_{lo} \approx 0.04\%$, $p_{hi} \approx 0.9\%$. The transition spans less than 1% in p_c , explaining the empirically observed cliff: methods that are stable at $p_c = 25\%$ (Protocol 1) can collapse catastrophically at $p_c = 0.07\%$ (Protocol 3), despite a seemingly modest change in the nominal missing rate.

Remark (scope and limitations). (i) The $1/p_c$ rate applies to the \mathcal{F}_{rec} recovery branch. Methods with a recovery-independent contrastive loss retain gradient signal from that branch, but the degenerated recovery module can actively contaminate the contrastive branch (Appendix B.5). (ii) Adaptive optimizers (Adam) maintain running gradient statistics that degrade under intermittent updates, potentially making the practical transition even sharper than the $1/p_c$ bound predicts. (iii) Stratified sampling that guarantees $B_c \geq 1$ per batch eliminates the zero-gradient issue, but the reduced effective batch size ($b_{eff} = Bp_c$) still inflates per-step variance by a factor of $1/p_c$. (iv) The premise “derive gradient exclusively from complete samples” is specific to \mathcal{F}_{rec} (Class 1) methods. Methods that train recovery modules through distributional objectives operating on per-view statistics (e.g., Energy-DIMC) retain gradient signal at $p_c = 0$ and are not subject to this bound; their degradation is instead governed by Theorem 4.1. \square

Remark (fixed-topology failure, ProImp case). The `cross_rec()` module of ProImp constructs tensors of shape $|C| \times K$ and $|C| \times |C|$. Under Protocol 4 with $V=2$ and $r \geq 0.5$, $|C| = 0$. The fallback produces shape $(1, 1)$ and $(1, K)$, while downstream operations expect (n, K) , triggering `RuntimeError: The size of tensor a (1) must match the size of tensor b (600)`. This is a direct consequence of the fixed-topology design: the architecture assumes a fixed number of complete samples and cannot adapt when that number reaches zero.

Remark (CRAFT avoids both failure modes). The computation graph for sample i involves only (i) its observed features $\{\mathbf{x}_v^{(i)} : v \in O_i\}$ and (ii) shared parameters θ . No features of any other sample or the global statistic p_c appear. Both training and inference proceed normally at $p_c = 0$. The Transformer’s self-attention matrix has dimensions determined by the actual token count $|O_i| + 1$ (including CLS); reducing the token count changes the matrix size but does not invalidate any operation.

B.2 Capability Bound: Theorem Statement and Proof

This subsection states and proves the capability bound referenced throughout the main text (§4, §6.2, §7). The bound limits the cluster-relevant information any clustering function can extract from a given observed-view subset, regardless of training dynamics or architecture, and applies to all methods including those outside \mathcal{F}_{rec} (e.g., distributional methods such as Energy-DIMC).

We prove Theorem 4.1 (statement in §4). When views are correlated beyond what Y explains, the upper bound is loose and the operational ceiling reduces to the lower bound.

Proof of Theorem 4.1. Upper bound. Under Assumption 4.1 (conditional independence of views given Y), the joint entropy decomposes as $H(\{X_v\}_{v \in O_i} | Y) = \sum_{v \in O_i} H(X_v | Y)$. By the subadditivity of entropy, $H(\{X_v\}_{v \in O_i}) \leq \sum_{v \in O_i} H(X_v)$. Therefore,

$$\begin{aligned} I(\{X_v\}_{v \in O_i}; Y) &= H(\{X_v\}_{v \in O_i}) - H(\{X_v\}_{v \in O_i} | Y) \\ &\leq \sum_{v \in O_i} H(X_v) - \sum_{v \in O_i} H(X_v | Y) \\ &= \sum_{v \in O_i} I(X_v; Y). \end{aligned} \tag{4}$$

Lower bound. For any $u \in O_i$, X_u is a component of $\{X_v\}_{v \in O_i}$. Adding more variables cannot decrease mutual information: $I(\{X_v\}_{v \in O_i}; Y) \geq I(X_u; Y)$. Taking the maximum over $u \in O_i$ gives the lower bound.

Application to fused representations. Since the fused representation $\mathbf{h}_{\text{cls}}^{(i)}$ is a deterministic function of $\{X_v\}_{v \in O_i}$, the data processing inequality gives $I(\mathbf{h}_{\text{cls}}^{(i)}; Y) \leq I(\{X_v\}_{v \in O_i}; Y)$. Combined with the lower bound, the fused representation carries at least $\max_{v \in O_i} I(X_v; Y)$ and at most $\sum_{v \in O_i} I(X_v; Y)$ information about Y . When $|O_i| = 1$ (as under $V=2$ Protocol 4 with $r \geq 0.5$), both bounds coincide and multi-view complementarity is forfeited—explaining the soft degradation observed for methods free of recovery gradient vanishing (e.g., Energy-DIMC drops from 65.23% to 42.38% on CUB at Protocol 2/4 transition). \square

B.3 Proof of Theorem 4.2 (Family-Local Necessity within \mathcal{F}_{rec})

This appendix proves Theorem 4.2 of the main text: within the family \mathcal{F}_{rec} of cross-view reconstruction losses, single-view trainability is structurally required for cross-protocol stability. The proof has three lemmas, each isolating one step of the chain: **(A)** expected per-step gradient magnitude is upper-bounded by the pairwise observation rate $q_2(P)$; **(B)** expected parameter trajectory is upper-bounded by $\eta T q_2(P)$; **(C)** small parameter displacement implies near-initialization clustering accuracy. The theorem follows by combining (A)–(C) with the gap between P_1 ’s converged accuracy and P_4 ’s near-initialization accuracy.

B.3.1 Notation and Setting

Let $\Theta \subseteq \mathbb{R}^p$ be the parameter space and $\theta_0 \in \Theta$ the initialization. We denote by f_θ the representation map and by $\hat{Y}_\theta : \mathcal{X}_S \rightarrow [K]$ the clustering output (for any observed-view set S).

Loss family \mathcal{F}_{rec} . A method’s training loss lies in \mathcal{F}_{rec} if it admits a per-sample decomposition

$$\mathcal{L}(\theta; \mathcal{D}, \mathbf{M}) = \frac{1}{n} \sum_{i=1}^n \mathbf{1}\{|O_i| \geq 2\} \cdot \tilde{\ell}(\theta; X^{(i)}, M^{(i)}), \quad (5)$$

where $\tilde{\ell}$ is the per-sample reconstruction loss, defined only when at least two views of sample i are observed (i.e., the indicator $\mathbf{1}\{|O_i| \geq 2\}$ vanishes the term when $|O_i| < 2$). This captures cross-view reconstruction methods in which the reconstruction loss is computed over pairs of views co-observed for the same sample (§2).

Protocol probabilities. For a protocol P (a distribution over M), define

$$q_k(P) := \mathbb{P}_{M \sim P} [|O| \geq k], \quad k \in \{1, \dots, V\}. \quad (6)$$

For full-view reconstruction ($k = V$), $q_V(P) = p_c(P)$, the complete-sample proportion. Throughout, we work with $q_2(P)$ since \mathcal{F}_{rec} requires only pairwise co-observation.

Cross-protocol ϵ -stability. A method $(\theta_0, \mathcal{L}, \mathcal{A})$, where \mathcal{A} is the optimization algorithm, is ϵ -stable on a protocol family \mathcal{P} at training budget T if

$$\sup_{P, P' \in \mathcal{P}} |\mathbb{E} \text{Acc}(\theta_T^P) - \mathbb{E} \text{Acc}(\theta_T^{P'})| \leq \epsilon, \quad (7)$$

where θ_T^P denotes the parameter after T SGD steps on data drawn under P , and the expectation is over training randomness and protocol-induced data sampling.

B.3.2 Assumptions

The proof uses three local assumptions on the loss landscape and the optimization process; all are mild and standard in non-convex optimization analyses.

Assumption B.1 (Bounded per-sample gradient). *There exists $C_g < \infty$ such that for all θ in a compact neighborhood $\mathcal{N}(\theta_0)$ containing the optimization trajectory, and almost all (X, M) with $|O| \geq 2$, $\|\nabla_\theta \tilde{\ell}(\theta; X, M)\| \leq C_g$.*

Assumption B.2 (Continuity of clustering accuracy in expectation). *There exists a non-decreasing concave modulus $\omega : [0, \infty) \rightarrow [0, \infty)$ with $\omega(0) = 0$ and $\lim_{u \rightarrow 0^+} \omega(u) = 0$ such that for all $\theta \in \mathcal{N}(\theta_0)$,*

$$|\mathbb{E} \text{Acc}(\theta) - \mathbb{E} \text{Acc}(\theta_0)| \leq \omega(\|\theta - \theta_0\|). \quad (8)$$

Concavity is standard for moduli of continuity (e.g., the Lipschitz, Hölder, and bounded-margin moduli all satisfy it).

Assumption B.3 (Convergence under sufficient signal). *There exists $q^* > 0$ and an accuracy gap $\Delta > 0$ such that for any protocol P with $q_2(P) \geq q^*$, applying T steps of SGD on \mathcal{L} yields $\mathbb{E} \text{Acc}(\theta_T^P) \geq \mathbb{E} \text{Acc}(\theta_0) + \Delta$.*

Discussion. Assumption B.1 rules out exploding gradients in the relevant region; it holds for the bounded-output reconstruction losses of COMPLETER, DCG, DCP, ProImp, APADC, and HSACC (§2). Assumption B.2 captures the fact that small parameter perturbations lead to small expected accuracy changes after marginalizing over data and label permutations (see [1] for related arguments in cluster-validity analysis); the modulus ω encodes how fast accuracy responds to parameter movement and is method/dataset-specific. Assumption B.3 asserts that for protocols providing non-trivial pairwise co-observation (here, P_1), the method actually trains to a non-trivial accuracy above initialization—a baseline-level requirement on any usable \mathcal{F}_{rec} method (validated empirically in §6.2 for P_1).

B.3.3 Lemma A: Gradient Magnitude Bound

Lemma B.1 (Gradient magnitude under protocol P). *Under Assumption B.1, for any $\theta \in \mathcal{N}(\theta_0)$ and any sample $i \sim \text{Unif}([n])$ with $M^{(i)} \sim P$ independent of past iterates,*

$$\mathbb{E}_{i, M^{(i)} \sim P} \|\nabla_{\theta} \ell_i(\theta)\| \leq C_g \cdot q_2(P). \quad (9)$$

Proof. By the definition of \mathcal{F}_{rec} in (5), $\nabla_{\theta} \ell_i(\theta) = \mathbf{1}\{|O_i| \geq 2\} \cdot \nabla_{\theta} \tilde{\ell}(\theta; X^{(i)}, M^{(i)})$. Therefore

$$\begin{aligned} \|\nabla_{\theta} \ell_i(\theta)\| &= \mathbf{1}\{|O_i| \geq 2\} \cdot \|\nabla_{\theta} \tilde{\ell}(\theta; X^{(i)}, M^{(i)})\| \\ &\leq \mathbf{1}\{|O_i| \geq 2\} \cdot C_g \quad (\text{Assumption B.1}). \end{aligned} \quad (10)$$

Taking expectation over i and $M^{(i)} \sim P$:

$$\mathbb{E} \|\nabla_{\theta} \ell_i(\theta)\| \leq C_g \cdot \mathbb{P}_{M^{(i)} \sim P}[|O_i| \geq 2] = C_g \cdot q_2(P). \quad \square$$

Remark. The bound is tight up to a factor of C_g/c_g when $\tilde{\ell}$ has uniformly lower-bounded gradient on its support (a stronger version of Assumption B.1). The upper bound suffices for the necessity argument; tightness is not needed.

B.3.4 Lemma B: Parameter Trajectory Bound

Lemma B.2 (Parameter displacement after T SGD steps). *Let θ_t evolve under SGD with constant step size $\eta > 0$: $\theta_{t+1} = \theta_t - \eta \nabla_{\theta} \ell_{i_t}(\theta_t)$, where $\{i_t\}$ are iid uniform on $[n]$ and $\{M^{(i_t)}\} \sim P$ iid. Suppose all $\theta_t \in \mathcal{N}(\theta_0)$ for $t \in [0, T]$. Then*

$$\mathbb{E} \|\theta_T - \theta_0\| \leq \eta T \cdot C_g \cdot q_2(P). \quad (11)$$

Proof. By the triangle inequality,

$$\begin{aligned} \|\theta_T - \theta_0\| &= \left\| \sum_{t=0}^{T-1} (\theta_{t+1} - \theta_t) \right\| = \left\| \sum_{t=0}^{T-1} \eta \nabla_{\theta} \ell_{i_t}(\theta_t) \right\| \\ &\leq \eta \sum_{t=0}^{T-1} \|\nabla_{\theta} \ell_{i_t}(\theta_t)\|. \end{aligned} \quad (12)$$

Taking expectation and applying Lemma B.1 to each term (using that the iterate θ_t is independent of the future sample $(i_t, M^{(i_t)})$ in the standard SGD analysis):

$$\mathbb{E} \|\theta_T - \theta_0\| \leq \eta \sum_{t=0}^{T-1} \mathbb{E} \|\nabla_{\theta} \ell_{i_t}(\theta_t)\| \leq \eta T \cdot C_g \cdot q_2(P). \quad (13) \quad \square$$

Remark on the assumption $\theta_t \in \mathcal{N}(\theta_0)$. This is automatic when $q_2(P)$ is small: the parameter cannot drift far from θ_0 when its expected per-step displacement is bounded by $\eta C_g q_2(P)$. Formally, choose $\mathcal{N}(\theta_0) = \{\theta : \|\theta - \theta_0\| \leq r_0\}$ with r_0 large enough that $\eta T C_g q_2(P) < r_0$ (which is the regime we care about). The assumption then reads as a constraint on T relative to $r_0/(\eta C_g q_2(P))$, which is automatically satisfied when $q_2(P)$ is small.

B.3.5 Lemma C: Accuracy Near Initialization

Lemma B.3 (Accuracy collapse to baseline under small displacement). *Under Assumption B.2, for any $\theta \in \mathcal{N}(\theta_0)$ satisfying $\mathbb{E}\|\theta - \theta_0\| \leq \delta$,*

$$|\mathbb{E} \text{Acc}(\theta) - \mathbb{E} \text{Acc}(\theta_0)| \leq \omega(\delta). \quad (14)$$

Proof. By Assumption B.2 applied pointwise (with the expectation taken over data) and Jensen's inequality (using concavity of ω over the random θ):

$$\begin{aligned} |\mathbb{E} \text{Acc}(\theta) - \mathbb{E} \text{Acc}(\theta_0)| &\leq \mathbb{E}_\theta |\mathbb{E}_X \text{Acc}(\theta) - \mathbb{E}_X \text{Acc}(\theta_0)| \\ &\leq \mathbb{E}_\theta \omega(\|\theta - \theta_0\|) \\ &\leq \omega(\mathbb{E}_\theta \|\theta - \theta_0\|) \quad (\text{Jensen, } \omega \text{ concave}) \\ &\leq \omega(\delta) \quad (\omega \text{ non-decreasing}). \quad \square \end{aligned}$$

Remark on cluster-assignment discreteness. Clustering accuracy involves a discrete assignment $\hat{Y}_\theta(x) \in [K]$, which is generally not Lipschitz in θ . Assumption B.2 sidesteps this by requiring continuity *in expectation*, where the expectation is taken over the data distribution. For models producing continuous logits with a argmax readout, the expectation smooths the discreteness on the boundary set, where logits are tied; this set has measure zero for almost-everywhere distinct random initialization. Sharper versions of Lemma B.3 under additional logit-margin assumptions are possible but not needed for our argument.

B.3.6 Proof of Theorem 4.2

Theorem B.1 (Family-local necessity within \mathcal{F}_{rec} , restated). *Let $\ell \in \mathcal{F}_{rec}$ satisfy Assumptions B.1–B.3. Suppose P_1, P_4 are protocols at the same nominal missing rate r such that $q_2(P_1) \geq q^*$ and $q_2(P_4) \leq \delta_0$, where δ_0 satisfies*

$$\omega(\eta T C_g \delta_0) < \Delta. \quad (15)$$

Then for any ϵ with

$$\epsilon < \Delta - \omega(\eta T C_g \delta_0), \quad (16)$$

the method is not ϵ -stable on $\{P_1, P_4\}$.

Proof. We bound the two protocols' expected accuracies separately.

Under P_1 . By Assumption B.3 applied to P_1 (which satisfies $q_2(P_1) \geq q^*$),

$$\mathbb{E} \text{Acc}(\theta_T^{P_1}) \geq \mathbb{E} \text{Acc}(\theta_0) + \Delta. \quad (17)$$

Under P_4 . By Lemma B.2,

$$\mathbb{E}\|\theta_T^{P_4} - \theta_0\| \leq \eta T C_g \cdot q_2(P_4) \leq \eta T C_g \delta_0. \quad (18)$$

By Lemma B.3 with $\delta = \eta T C_g \delta_0$,

$$|\mathbb{E} \text{Acc}(\theta_T^{P_4}) - \mathbb{E} \text{Acc}(\theta_0)| \leq \omega(\eta T C_g \delta_0). \quad (19)$$

Combining (17) and (19).

$$\begin{aligned} \mathbb{E} \text{Acc}(\theta_T^{P_1}) - \mathbb{E} \text{Acc}(\theta_T^{P_4}) &\geq (\mathbb{E} \text{Acc}(\theta_0) + \Delta) - (\mathbb{E} \text{Acc}(\theta_0) + \omega(\eta T C_g \delta_0)) \\ &= \Delta - \omega(\eta T C_g \delta_0). \end{aligned} \quad (20)$$

By (16), this exceeds ϵ :

$$|\mathbb{E} \text{Acc}(\theta_T^{P_1}) - \mathbb{E} \text{Acc}(\theta_T^{P_4})| > \epsilon, \quad (21)$$

contradicting ϵ -stability of the method on $\{P_1, P_4\}$. \square

B.3.7 Scope, Boundary, and Honest Limits

We discuss three boundary conditions where Theorem 4.2 does not directly apply, justifying the family-local qualifier.

(B1) Methods outside \mathcal{F}_{rec} . The decomposition (5) is essential to Lemma B.1: without the indicator $\mathbf{1}\{|O_i| \geq 2\}$, $\nabla \ell_i$ need not vanish for samples with $|O_i| = 1$ or $|O_i| = 0$. Methods whose loss does not pre-zero on $|O_i| < 2$ —for example, distributional losses (Energy-DIMC, [24]) and contrastive losses invariant to observation patterns (SimSiam-style [3] consistency)—are not covered by the bound. Their failure modes are characterized by Theorem 4.1 (capability bound) instead of Proposition 4.1 (trainability bound), as discussed in §4.

(B2) Higher-order optimizers and large batches. The argument uses constant-step SGD with iid samples. For Adam, RMSProp, and similar adaptive optimizers, the gradient bound in Lemma B.1 still holds, but the trajectory bound in Lemma B.2 loosens by a factor depending on the optimizer’s effective step-size adaptation. For mini-batches of size B , $q_2(P)$ in Lemma B.1 is replaced by $1 - (1 - q_2(P))^B$; when $q_2(P) \rightarrow 0$, this still vanishes for fixed B , preserving the conclusion. Empirically (§6.2), the methods studied use Adam with $B \in \{64, 256\}$ and exhibit the predicted collapse, suggesting the result extends qualitatively.

(B3) Non-degeneracy of $\tilde{\ell}$. Assumption B.1 rules out gradient explosion but does not address pathological loss landscapes (e.g., $\tilde{\ell}$ identically zero on its support). Such pathologies do not occur for standard reconstruction losses (ℓ_2 , cross-entropy, contrastive) used by \mathcal{F}_{rec} methods.

Sharpness of the bound. The bound $\eta TC_g q_2(P)$ in Lemma B.2 is tight up to constants when $\tilde{\ell}$ has uniformly lower-bounded gradient on its support and the optimization trajectory stays within a region of bounded curvature. The conclusion of Theorem 4.2 is therefore sharp in its dependence on $q_2(P)$: methods with loss family \mathcal{F}_{rec} *must* have parameter movement proportional to $q_2(P)$, and any non-trivial accuracy improvement requires $q_2(P)$ above a method-dependent threshold.

B.3.8 Why “Family-Local” Is Not a Weakness

A natural reaction to Theorem 4.2 is to ask whether necessity can be extended beyond \mathcal{F}_{rec} to all unstable methods. The answer is no, by construction: there exist methods that violate the strict per-sample, single-view-trainable form yet remain protocol-stable. As an illustration, consider a contrastive consistency loss $\ell_i^{\text{sim}}(\theta) = \|h^{(i)} - \text{sg}(h^{(j)})\|^2$ over a randomly sampled pair (i, j) , where sg is the stop-gradient operator. This loss is non-zero for any $|O_i| \geq 1$, $|O_j| \geq 1$, and its expected gradient depends on the marginal distribution of h , which is itself only a function of $|O|$ (under permutation-equivariant fusion). Such methods can be cross-protocol stable while violating the strict \mathcal{F}_{rec} form.

The family-local result is therefore not a weakening of an aspirational “full necessity” theorem but the correct scoping: it characterizes the boundary of stable methods *within the dominant IMVC paradigm of cross-view reconstruction*, which is what practitioners and benchmark authors most need to know. Methods outside \mathcal{F}_{rec} require the separate analysis carried out in §2 and §4, anchored on Theorem 4.1 (capability) and Assumption 4.1 (conditional independence).

B.4 Cluster-Information Bound: Y is the Statistical Bridge

Corollary B.1 (Recovery does not increase available information at inference). *Let $\hat{X}_v = g_\phi(\{X_u\}_{u \in O_i})$ be the output of a recovery module applied to the observed views at inference. Then $I(\{X_u\}_{u \in O_i}, \hat{X}_v; Y) = I(\{X_u\}_{u \in O_i}; Y)$.*

Proof. Direct from the data processing inequality: \hat{X}_v is a deterministic function of $\{X_u\}_{u \in O_i}$, so appending it to the conditioning set cannot increase information about Y . \square

This concerns inference-time information content. During training, recovery modules provide a useful gradient signal through cross-view reconstruction, formalized below.

Proposition B.1 (Cross-view reconstruction as implicit cluster-information maximization). *Under Assumption 4.1, for any encoder f_θ and any two views u, v :*

$$I(f_\theta(X_u); X_v) \leq I(f_\theta(X_u); Y). \quad (22)$$

Consequently, any training objective that increases $I(f_\theta(X_u); X_v)$ —including cross-view reconstruction losses—implicitly increases $I(f_\theta(X_u); Y)$.

Proof. Since $f_\theta(X_u)$ is a deterministic function of X_u , and $X_u \perp X_v \mid Y$ by Assumption 4.1, $f_\theta(X_u) \perp X_v \mid Y$, giving $I(f_\theta(X_u); X_v \mid Y) = 0$. Applying the chain rule:

$$\begin{aligned} I(f_\theta(X_u); X_v) &= I(f_\theta(X_u); X_v, Y) - I(f_\theta(X_u); Y \mid X_v) \\ &\leq I(f_\theta(X_u); X_v, Y) \\ &= I(f_\theta(X_u); Y) + \underbrace{I(f_\theta(X_u); X_v \mid Y)}_{=0}. \quad \square \end{aligned}$$

Interpretation. Eq. (22) says that the cross-view predictive information is bounded above by the cluster-relevant information. Under conditional independence, Y is the sole statistical bridge between X_u and X_v : any feature of X_u that is predictive of X_v must pass through Y . A reconstruction loss that pushes $I(f_\theta(X_u); X_v)$ upward can only do so by forcing f_θ to extract more information about Y . This explains why CRAFT’s Stage 1 reconstruction loss is effective despite targeting already-observed views: under Assumption 4.1, the reconstruction objective *is* implicit cluster-information maximization.

B.5 Attention Reweighting and Exact Exclusion

Proposition B.2 (Attention Leakage Bound for Placeholder Tokens). *When absent views are replaced by learnable placeholder tokens with bounded logits $\leq \varepsilon$, the total attention weight assigned to k absent positions satisfies*

$$\sum_{j \in \text{mask}} \alpha_j \leq \frac{k}{V - k} \cdot \exp(\varepsilon - s_{\min}).$$

Proof. The mask set has k elements with scaled dot product $\leq \varepsilon$: $\sum_{j \in \text{mask}} \exp(\mathbf{q}^\top \mathbf{k}_j / \sqrt{d}) \leq k \cdot \exp(\varepsilon)$. The denominator $Z \geq (V - k) \cdot \exp(s_{\min})$. Dividing yields the claim. \square

Corollary (Exact exclusion under attention masking). Under canonical CRAFT, $\varepsilon = -\infty$ (attention masking sets the logit to $-\infty$ before the softmax) and the bound yields $\sum_{j \in \text{mask}} \alpha_j = 0$ exactly. This guarantees that absent views contribute zero information to the fused representation, ensuring smooth degradation rather than discontinuous collapse and giving strict satisfaction of C2.

Empirical verification. On HandWritten ($V=6$) with $k=1$, the learnable-placeholder variant allocates 9.4% of CLS attention to the placeholder versus the 16.7% uniform share, confirming that the trained model systematically aligns real-token keys more closely with the CLS query but does not achieve exact exclusion—only canonical attention masking does.

B.6 MFT as Weighted View-Subset Ensemble

Proposition B.3 (View Dropout Ensemble). *In MFT, each sample draws $k \sim \text{Uniform}(\{0, \dots, V-2\})$ views to exclude. The expected MFT loss equals a weighted sum over view subsets:*

$$\mathbb{E}_{\mathbf{m}}[\mathcal{L}(f_\theta(\mathbf{x}, \mathbf{m}))] = \sum_{S: |S| \geq 2} P(S) \cdot \mathcal{L}(f_\theta(\mathbf{x}_S)),$$

where $P(S) = 1 / ((V-1) \binom{V}{V-|S|})$.

Proof. Each mask determines a unique retained subset. The probability of a specific subset S with $|S| = V - k$ is $\frac{1}{V-1} \cdot \frac{1}{\binom{V}{k}}$. Normalization is verified by $\sum_{k=0}^{V-2} \binom{V}{k} / ((V-1) \binom{V}{k}) = 1$. \square

Interpretation. (1) The full-view subset ($k=0$) appears with probability $1/(V-1)$, preserving complete-data performance. (2) At $V=6$, 57 distinct subsets participate in the ensemble, providing strong regularization; at $V=2$, only 1 subset (full data) participates, explaining why MFT has no benefit on CUB (§6.3). (3) With weak base models, all sub-models perform poorly and ensemble aggregation cannot compensate, explaining MFT’s failure on datasets with low base accuracy.

C Protocol Analysis

C.1 Closed-Form Protocol Formulas

For each protocol introduced in §3.2, we state the closed-form expressions for the realized entry-wise missing rate \hat{r} and the complete-sample proportion p_c in the limit $n \rightarrow \infty$. Throughout, $r \in [0, 1]$ denotes the nominal missing rate as reported by each method.

Protocol 1 (sample-level; delete one view per sample). A fraction r of samples are designated incomplete; for each incomplete sample, exactly one view is deleted uniformly at random. Then:

$$\hat{r}_{P1} = \frac{r}{V}, \quad p_c^{P1} = 1 - r.$$

Protocol 2 (protected view; entry-wise at r/V). For each sample, exactly one view is randomly designated as “protected” (always observed); the remaining $V-1$ views are masked by independent Bernoulli($r/(V-1)$) trials, calibrated to realize the nominal entry-wise rate r/V in expectation. Then:

$$\hat{r}_{P2} = \frac{r}{V}, \quad p_c^{P2} = \left(1 - \frac{r}{V-1}\right)^{V-1}.$$

Protocol 3 (entry-wise Bernoulli at r ; one-hot guarantee). Each entry $M_v^{(i)}$ is masked by an independent Bernoulli(r) trial; any sample that loses all V views has one randomly chosen view restored (the one-hot guarantee). Then:

$$\hat{r}_{P3} = r - \frac{r^V}{V}, \quad p_c^{P3} = (1 - r)^V.$$

Protocol 4 (protected view; exact entry-wise at r). For each sample, one protected view is fixed; the remaining $V-1$ views are masked deterministically to realize an entry-wise missing rate of exactly r (subject to the cap $\hat{r} \leq (V-1)/V$ enforced by the protected view). The limit derivation through binomial sampling on the $V-1$ non-protected positions yields:

$$\hat{r}_{P4} = \min\left(r, \frac{V-1}{V}\right), \quad p_c^{P4} = \max\left(0, \left(1 - \frac{Vr}{V-1}\right)^{V-1}\right).$$

Numerical separation. At low r , the four formulas for p_c are nearly indistinguishable ($p_c \rightarrow 1$ as $r \rightarrow 0$). At moderate-to-high r and $V \geq 3$, they diverge by orders of magnitude—e.g., on $V=6$, $r=0.7$: $p_c^{P1} = 30\%$ vs. $p_c^{P4} \approx 1.0 \times 10^{-4}$, a $\sim 3,000\times$ gap at the same nominal rate. Numerical instantiations appear in Table 5.

C.2 Monte Carlo Verification of Protocol Formulas

We verify the closed-form expressions for \hat{r} and p_c through Monte Carlo simulation ($n=2000$, $V=6$, 100 independent trials per combination). Empirical means match analytical predictions within 0.5% in all cases.

Protected-view ceiling. The protected view imposes an upper bound of $(V-1)/V$ on \hat{r} under Protocol 4. When $V=2$, $r=0.5$ and $r=0.7$ generate identical mask matrices. When $V=3$, the ceiling is $2/3 \approx 0.667$, so $r=0.7$ cannot be fully realized. High-missing-rate experiments on two-view datasets carry no discriminative power under this protocol.

DSIMVC protocol equivalence. DSIMVC uses per-sample Bernoulli trials rather than the fixed-count sampling of Protocol 1. By the law of large numbers, the fraction of incomplete samples converges to r as $n \rightarrow \infty$; for $n=2000$, the standard deviation is $\sqrt{r(1-r)/n} < 1.2\%$. The two procedures produce statistically indistinguishable mask matrices at the dataset sizes used in our experiments.

C.3 Hidden-Variable Numerical Profiles

Table 5 instantiates the closed-form expressions for two representative configurations.

Table 5: Hidden variables (\hat{r} and p_c) under four protocols, computed from the limiting formulas in §C.1.

Protocol	$V=2, r=0.5$		$V=6, r=0.7$	
	\hat{r}	p_c	\hat{r}	p_c
1	25.0%	50.0%	11.7%	30.0%
2	25.0%	50.0%	11.7%	47.0%
3	37.5%	25.0%	68.0%	0.073%
4	50.0%	0%	70.0%	0.010%

The right-hand block ($V=6, r=0.7$) exhibits a $\sim 4500\times$ divergence in p_c between Protocol 2 (47%) and Protocol 4 (0.010%) at the same nominal missing rate—the empirical manifestation of the trainability-vs- capability separation analyzed in §4. Even the intermediate comparison Protocol 2 vs. Protocol 3 (47% vs. 0.073%) shows a $640\times$ divergence.

C.4 Protocol Mappings in Nine Implementations

To determine which protocol each method actually uses, we inspected the official code repositories of nine IMVC methods published between 2021 and 2025. Table 6 records the masking mechanism observed in each implementation and identifies the closest matching protocol from §C.1.

The realized protocol distribution is concentrated: **seven of nine methods** sit at Protocol 2, and **the remaining two** (DSIMVC, DVIMC) at Protocol 1. The stricter regimes (Protocols 3 and 4) are not exercised by any existing IMVC implementation prior to this work; this absence is precisely the coverage gap that produces the cliff observed in §6.2 when methods built on Protocol 2 assumptions are evaluated under Protocol 4.

D Complete Experimental Results

D.1 CUB ($V=2$)

CRAFT uses one canonical checkpoint ($\lambda_{\text{repr}}=0.1, \tau=0.1$, no MFT); baselines retrain per configuration. Under Protocol 4 with $V=2$ the protected view caps \hat{r} at 0.5, so Protocol 4 $r=0.7$ reproduces the $r=0.5$ masks (§C.2).

D.2 HandWritten ($V=6$)

Per-(protocol, rate) accuracy on HandWritten under canonical CRAFT (Stage 1 + Stage 2 + MFT, per §6.1); baselines retrain per configuration, CRAFT trains once on complete data.

D.3 MultiFashion ($V=3$)

Table 9 reports per-(protocol, r) accuracy on MultiFashion; baselines retrain per configuration, CRAFT trains once on complete data with MFT enabled at $V\geq 3$.

D.4 UCI-Digit, Out-Scene, and Caltech

A single CRAFT checkpoint per dataset is evaluated across all 16 (protocol, r) configurations, mirroring the train-once protocol in §6.1; Table 10 reports the results. Baselines were not re-run on these three supplementary benchmarks.

The same pattern holds on all three benchmarks: lenient protocols (P1, P2) stay nearly flat as r grows, while stringent protocols (P3, P4) expose the genuine p_c -driven degradation. Caltech’s larger Proto. 4 variance at $r=0.7$ (± 4.5) reflects its heterogeneous view dimensions and the shallow encoder necessitated by the high-dimensional GIST view.

Table 6: Masking mechanism in nine IMVC implementations, mapped to the closest protocol from §C.1. ‡ shared masking code; † per-sample Bernoulli vs. fixed-count (§C.2); + Protocol 2 with a deterministic complete-sample floor.

Method	Venue	Masking Mechanism	Proto.
COMPLETER‡ [13]	CVPR’21	r/V entry-wise + protected view + calibration	2
DCP‡ [14]	TPAMI’22	r/V entry-wise + protected view (shared codebase)	2
DSIMVC	ICML’22	per-sample Bernoulli, post-fix $ O_i \geq 1$	1†
ProImp‡ [11]	IJCAI’23	r/V entry-wise + protected view	2
APADC‡ [30]	TIP’23	r/V entry-wise + protected view	2
DVIMC [2]	AAAI’24	sample-level; delete $1 \sim V-1$ views per incomplete sample	1
DCG‡ [34]	AAAI’25	r/V entry-wise + protected view	2
Energy-DIMC [24]	MM’25	μ/V entry-wise + per-sample protected view	2
HSACC [5]	NeurIPS’25	$(1-r)n$ complete samples + entry-wise masking on rest	2+

Table 7: ACC (%) on CUB ($V=2, K=10$). †Protocol 4 $r=0.7$ reproduces $r=0.5$ masks. *BURG cited from original paper.

Method	r	Proto. 1	Proto. 2	Proto. 3	Proto. 4
DCG	0.1	71.50	74.11	70.50	70.28
	0.3	72.56	70.33	67.78	65.39
	0.5	73.33	69.11	60.17	15.61
	0.7	63.50	59.16	55.95	17.72
COMPLETER	0.1	51.33	55.80	63.23	61.23
	0.3	61.60	62.43	52.10	18.27
	0.5	49.83	53.67	19.43	36.43
	0.7	18.90	18.50	21.13	36.43
DCP	0.1	65.00	59.83	62.33	64.17
	0.3	57.50	62.67	44.83	29.67
	0.5	51.33	51.83	28.17	36.83
	0.7	26.00	27.00	34.33	36.83
Energy-DIMC	0.1	75.20	68.55	71.48	71.29
	0.3	67.77	74.61	65.62	53.52
	0.5	58.20	65.23	47.85	42.38
	0.7	51.56	59.77	45.51	42.38
BURG*	0.1	—	71.50	—	—
	0.3	—	58.00	—	—
	0.5	—	57.33	—	—
	0.7	—	53.83	—	—
HSACC	0.1	63.13±1.2	63.63±2.2	62.23±2.4	59.50±2.3
	0.3	54.00±3.2	57.20±4.1	45.03±4.0	33.13±1.9
	0.5	43.40±3.2	45.63±3.1	30.70±0.6	38.63±1.5
	0.7	29.67±0.5	30.67±1.4	35.00±0.6	38.63±1.5
CRAFT	0.1	82.09±1.0	82.35±0.9	80.92±1.2	80.89±1.2
	0.3	79.19±1.1	79.44±1.3	76.27±1.6	74.15±2.2
	0.5	76.04±2.2	76.41±1.9	72.29±2.4	68.99±3.8
	0.7	73.61±2.7	73.23±2.7	69.81±2.9	68.99±3.8†

D.5 YTF-31 ($V=5, K=31$)

Table 11 reports per-(protocol, r) accuracy on YTF-31; the train-once advantage compresses a 16-run DCP grid (~ 16 hours) into a single CRAFT run (~ 3 hours).

D.6 Missing-Rate-Matched Training

To verify that CRAFT’s robustness is architectural (per-sample independence + variable-length fusion) rather than an artifact of training on complete data, we train a variant exposed to the target missing rate during training, using hyperparameters appropriate for this training regime (§6.1).

Table 8: ACC (%) on HandWritten ($V=6, K=10$). 5-seed mean \pm std. \dagger BURG cited from original paper.

Method	r	Proto. 1	Proto. 2	Proto. 3	Proto. 4
DCP	0.1	82.35	82.30	79.95	82.10
	0.3	83.90	84.00	22.45	24.60
	0.5	80.00	93.65	18.15	18.15
	0.7	71.55	70.10	16.40	16.25
Energy-DIMC	0.1	96.65	96.26	96.43	96.09
	0.3	96.37	96.54	95.20	94.87
	0.5	96.09	96.09	92.24	92.75
	0.7	96.37	95.65	83.98	83.26
BURG \dagger	0.1	—	95.70	—	—
	0.3	—	95.30	—	—
	0.5	—	94.30	—	—
	0.7	—	79.75	—	—
HSACC	0.1	76.53 \pm 3.7	80.48 \pm 8.6	87.89 \pm 7.4	89.39 \pm 1.3
	0.3	87.91 \pm 4.2	85.40 \pm 4.1	14.92 \pm 0.2	15.05 \pm 0.2
	0.5	87.10 \pm 5.0	84.10 \pm 5.8	14.08 \pm 0.5	14.24 \pm 0.2
	0.7	80.56 \pm 1.7	83.48 \pm 1.3	13.80 \pm 0.1	13.52 \pm 0.6
CRAFT	0.1	97.60 \pm 0.8	97.61 \pm 0.8	97.49 \pm 0.9	97.53 \pm 0.8
	0.3	97.57 \pm 0.8	97.59 \pm 0.8	96.51 \pm 0.9	96.82 \pm 0.8
	0.5	97.57 \pm 0.8	97.53 \pm 0.8	92.92 \pm 1.3	93.69 \pm 1.1
	0.7	97.58 \pm 0.9	97.49 \pm 0.9	86.03 \pm 2.1	85.21 \pm 2.4

Table 9: ACC (%) on MultiFashion ($V=3, K=10$). CRAFT uses attention masking with MFT; 5-seed mean.

Method	r	Proto. 1	Proto. 2	Proto. 3	Proto. 4
DCP	0.1	86.04	74.92	72.57	75.24
	0.3	72.75	75.21	66.18	67.21
	0.5	72.26	80.46	63.78	69.36
	0.7	68.95	78.73	33.21	25.11
Energy-DIMC	0.1	93.30	93.88	91.20	91.97
	0.3	91.64	91.27	87.75	88.53
	0.5	90.19	90.38	83.09	79.77
	0.7	89.90	89.61	72.60	29.14
HSACC	0.1	97.46 \pm 0.8	98.00 \pm 0.2	96.02 \pm 0.2	94.34 \pm 3.5
	0.3	96.40 \pm 0.3	96.29 \pm 0.1	85.17 \pm 3.8	82.50 \pm 2.5
	0.5	91.67 \pm 3.9	94.33 \pm 0.4	65.48 \pm 2.8	49.80 \pm 1.6
	0.7	83.36 \pm 3.0	88.03 \pm 3.6	17.62 \pm 1.3	21.61 \pm 0.4
DVIMC	0.1	83.86	86.51	79.95	86.65
	0.3	86.62	88.67	83.51	84.09
	0.5	88.82	85.81	80.67	80.43
	0.7	87.21	84.87	74.42	—
CRAFT	0.1	93.21	93.20	92.73	92.73
	0.3	92.82	92.70	90.66	90.83
	0.5	92.44	92.11	88.67	88.12
	0.7	91.97	91.38	86.64	85.41

Across the 8 configurations of Table 12, the two variants differ by at most 2.91pp; the per-rate variant occasionally outperforms complete-trained at the most stringent configurations (Protocol 4, $r \geq 0.5$). Both regimes confirm that CRAFT’s robustness stems from per-sample independence rather than from any particular training data distribution.

Table 10: CRAFT ACC (%) on UCI-Digit ($V=3, K=10$), Out-Scene ($V=4, K=8$), and Caltech ($V=6, K=20$). 5-seed mean \pm std.

Dataset	r	Proto. 1	Proto. 2	Proto. 3	Proto. 4
UCI-Digit	0.1	90.94 \pm 0.6	90.87 \pm 0.5	90.22 \pm 0.4	90.17 \pm 0.5
	0.3	90.59 \pm 0.4	90.08 \pm 0.3	85.75 \pm 1.8	85.61 \pm 1.9
	0.5	90.34 \pm 0.3	89.12 \pm 0.5	79.12 \pm 4.0	77.65 \pm 4.3
	0.7	90.14 \pm 0.6	87.64 \pm 1.1	72.93 \pm 5.9	68.31 \pm 6.9
Out-Scene	0.1	75.05 \pm 1.7	75.06 \pm 1.6	74.46 \pm 1.6	74.47 \pm 1.5
	0.3	74.61 \pm 1.5	74.69 \pm 1.6	71.34 \pm 1.7	71.49 \pm 1.6
	0.5	74.53 \pm 1.6	74.18 \pm 1.7	66.09 \pm 1.9	65.86 \pm 1.9
	0.7	74.07 \pm 1.8	73.60 \pm 1.5	59.78 \pm 2.1	57.05 \pm 2.1
Caltech	0.1	57.92 \pm 1.7	57.88 \pm 1.7	57.63 \pm 1.8	57.62 \pm 1.8
	0.3	57.78 \pm 1.8	57.77 \pm 1.7	56.17 \pm 2.1	56.23 \pm 2.0
	0.5	57.58 \pm 1.7	57.63 \pm 1.8	53.31 \pm 2.9	53.59 \pm 2.7
	0.7	57.40 \pm 1.7	57.35 \pm 1.8	48.12 \pm 4.5	47.74 \pm 4.5

Table 11: ACC (%) on YTF-31 ($V=5, K=31$). Random baseline: 3.2%. DCP trains 16 times (~ 16 hours); CRAFT trains once (~ 3 hours). Single seed (seed 42) due to dataset scale ($n \approx 100k$).

Method	r	Proto. 1	Proto. 2	Proto. 3	Proto. 4
DCP	0.1	32.97	33.29	27.95	33.85
	0.3	29.49	30.86	16.00	12.73
	0.5	28.05	33.04	10.80	11.17
	0.7	27.57	30.66	5.79	6.08
CRAFT	0.1	27.64	27.56	26.01	25.98
	0.3	26.88	26.76	22.39	22.27
	0.5	26.13	25.93	19.68	19.45
	0.7	25.39	25.16	18.45	18.10

D.7 Complete-MVC Comparison

CRAFT matches dedicated complete-MVC methods within a couple of percent on the two datasets where complete-MVC baselines have published numbers (Table 13), while uniquely providing robustness to arbitrary missing patterns that no existing complete-MVC method offers.

D.8 Training Time Details

CRAFT trains once on complete data and infers every (protocol, r) configuration, while baselines retrain per configuration. On MultiFashion, this collapses a 16-run \times 8-minute retraining grid into a single 14.5-minute run—the 8.8 \times wall-clock advantage quoted in the main text. The pattern scales: on YTF-31, 16 hours of DCP retraining is replaced by a single ~ 3 -hour CRAFT run.

D.9 Extended Trainability Collapse Verification

Trainability isolation configuration. Table 14 reports a controlled configuration on HandWritten designed to orthogonally isolate \hat{r} from p_c : Setting C uses Protocol 1 at $r=1$, in which every sample drops exactly one view, giving $\hat{r}=1/V \approx 16.67\%$ (close to the lenient Setting A) but $p_c = 0$ exactly (matching the stringent Setting D). Setting A and Setting C therefore share near-identical \hat{r} but differ in p_c by 30 percentage points, while Setting C and Setting D share $p_c \rightarrow 0$ but differ in \hat{r} by a factor of four. The vertical A \rightarrow C contrast isolates p_c as the causal driver, and the horizontal C \rightarrow D contrast confirms that varying \hat{r} at vanishing p_c does not alter the \mathcal{F}_{rec} collapse. Class-2 (Energy-DIMC) and Class-3 (CRAFT, CRAFT-Core) methods retain accuracy across all three settings; the bare C1+C2 minimum (CRAFT-Core, Stage 1 only) already escapes the trainability bound, and canonical CRAFT preserves its Setting A accuracy on Setting C without retraining.

\mathcal{F}_{rec} sub-families and the COMPLETER multi-view extension. \mathcal{F}_{rec} methods differ in whether their training loss requires fully-complete samples ($|O_i| = V$) or only pairwise co-observation ($|O_i| \geq 2$). DCP and DCG belong to the former; their effective q in Proposition 4.1 reduces to

Table 12: HandWritten ($V=6$): complete-trained vs. rate-matched CRAFT under Protocol 1 and Protocol 4. Both variants disable masked fine-tuning to ensure a configuration-matched comparison; the canonical CRAFT row in Table 2 enables MFT and reports higher accuracy (MFT helps at $V \geq 3$, see §6.3). † = single-seed evaluation; all other entries are 5-seed mean.

r	Protocol 1				Protocol 4			
	0.1	0.3	0.5	0.7	0.1	0.3	0.5	0.7
Complete-trained	97.37	97.50	97.69	97.83	97.48	95.68	90.56	82.48
Per-rate	94.75	94.59†	94.99	95.03	94.92	93.98	91.05	82.56
Gap	+2.62	+2.91	+2.70	+2.80	+2.56	+1.70	-0.49	-0.08

Table 13: Complete-data clustering performance (ACC %). † = numbers cited from original papers; OOM = out of memory on a single RTX 3090 (24 GB); — = not run.

Method	CUB	MF	UCI	OS	HW	Cal	YTF
EPFMVC†	—	—	—	—	96.90	—	—
SparseMVC [15]	77.07±1.1	OOM	90.27±3.5	77.49	90.26±3.5	47.10±1.1	OOM
CRAFT	83.80±1.1	93.41±0.3	91.46±0.5	75.55±0.8	97.49±0.9	58.86±1.2	28.10

p_c , predicting collapse on Setting C ($p_c = 0$) as observed in Table 14. The multi-view extension of COMPLETER used in this work instead adopts pairwise-complete training (reconstruction and prediction losses are computed on any view pair (i, j) for which both views are observed in a given sample). Under Min-1 (every sample retains $V-1$ views), each sample contributes $\binom{V-1}{2}$ co-observed view pairs and the relevant q remains $q_2(P) \approx 1$; Proposition 4.1 therefore does not predict collapse, and we empirically observe COMPLETER (5-seed) retains $68.76 \pm 5.34\%$ on Setting C. We omit COMPLETER from Table 14 as it represents a distinct trainability sub-family within \mathcal{F}_{rec} , not a counterexample to the bound.

Per-baseline failure modes (CUB Protocol 4, $r=0.5$). Table 15 matches each baseline’s observed behavior at this configuration to its predicted failure mode.

Energy-DIMC four-protocol comparison (HandWritten, $r=0.7$). CRAFT leads at every protocol on HandWritten (Table 16), but the gap narrows under stringent protocols: from $\sim 1.2\%$ at Protocol 1 to $\sim 1.95\%$ at Protocol 4. The narrowing is consistent with Theorem 4.1: Energy-DIMC’s distributional training signal is not p_c -bound, so at extreme missingness on high- V datasets where most samples retain a single high-information view, the capability ceiling dominates and the gap between strict-C2 architectures shrinks toward the shared ceiling.

D.10 Full Comparison with BURG

Under Protocol 2—BURG’s inferred protocol (§A.3.4)—CRAFT leads BURG at every tested rate on CUB and stays within $\sim 0.2\%$ of its lenient ceiling on HandWritten across r , while BURG itself develops a $\sim 15\%$ cliff between $r=0.5$ and $r=0.7$ on HandWritten (full per-rate numbers in Table 7 and Table 8).

D.11 Fusion Architecture Spectrum (Full Tables)

Table 17 reports the architectural variant comparison summarized in §6.2 across all four protocols on HandWritten ($V=6$). The variants share per-view encoders + Stage 1 + Stage 2 training without MFT to isolate fusion-architecture effects, differing only in the fusion block: (i) Transformer with attention masking (canonical CRAFT, strict C2); (ii) *SetMLP*, a DeepSets-style fusion [33] consisting of a per-view shared MLP, a masked mean pool over observed views, and a post-pool MLP of hidden dimension h' (strict C2), evaluated at two capacity tiers *SetMLP-Light* ($h'=d$, matching the per-dataset embedding dimension) and *SetMLP-Match* ($h'=560$, fixed across datasets); and (iii) a zero-fill concat fusion baseline (soft C2). DVIMC (hard C2) is omitted because its K-Means initialization fails when $|O_i| = 0$ (Appendix A.3.5). Canonical CRAFT in Table 8 adds MFT on top of (i). 5-seed mean \pm std.

Table 14: Trainability isolation on HandWritten ($V=6$, $K=10$). Setting A and Setting C share near-identical \hat{r} but differ in p_c from 30% to 0; Setting C and Setting D share $p_c \rightarrow 0$ but \hat{r} differs by a factor of 4. ACC (%); Setting C entries are 5-seed mean \pm std for Min-1; other settings are single-seed unless marked with std. Bold = best per setting; $\ddagger \leq 40\%$ on $K=10$; \dagger on a method name = single-seed evaluation; — = not run.

	Setting A Proto 1, $r=0.7$ $\hat{r}=11.7\%$ $p_c=30\%$	Setting C Proto 1, $r=1.0$ $\hat{r}\approx 16.67\%$ $p_c=0$	Setting D Proto 4, $r=0.7$ $\hat{r}=70\%$ $p_c\approx 0$
<i>Class 1: \mathcal{F}_{rec}</i>			
DCP [14]	71.55	19.79 $\pm 2.42^{\ddagger}$	16.25 ‡
DCG † [34]	62.30	12.29 $\pm 0.42^{\ddagger}$	12.75 ‡
<i>Class 2: cross-sample</i>			
Energy-DIMC [24]	96.37	94.14 ± 1.07	83.26
<i>Class 3: per-sample (C1+C2)</i>			
CRAFT-Core (Stage 1 only)	—	89.75	54.83
CRAFT (canonical)	97.58	96.34	85.21

Table 15: CUB, Protocol 4, $r=0.5$ ($p_c=0$). Observed failure modes match the predictions of Proposition 4.1 and the capability bound of Theorem 4.1. Bold = best ACC.

Method	ACC (%)	Predicted Behavior
DCG	15.61	Recovery gradient vanishes (Prop. 4.1)
ProImp	crash	Fixed-topology crash
COMPLETER	36.43	Partial recovery dependence
DCP	36.83	Partial recovery dependence
HSACC	38.63 ± 1.5	Partial recovery dependence
Energy-DIMC	42.38	No p_c dependence; capability bound (Thm. 4.1)
CRAFT	68.99± 3.8	Per-sample independence + variable-length fusion

Three findings. (1) *Architecture dominance.* The canonical Transformer dominates both SetMLP tiers and the fixed-input concat fusion baseline across every (protocol, rate) configuration, with the gap widening monotonically under stringent regimes; at the hardest tested condition the three strict-C2 architectures and the soft-C2 violator span $\sim 22\%$. (2) *Capacity is not the confound.* Doubling SetMLP’s hidden size from $h'=192$ to $h'=560$ (parameters comparable to the concat fusion baseline) does not narrow the gap to the Transformer; the larger SetMLP-Match *underperforms* the smaller SetMLP-Light by 5–7% under hard missingness. Putting more parameters into the wrong architecture moves performance *away* from CRAFT, ruling out the capacity-confound hypothesis. (3) *Soft-C2 leakage scales with r .* Within fixed-cardinality concat fusion, the zero-fill leakage compounds monotonically: SetMLP-Light’s lead over the fixed-input concat fusion baseline grows from a fraction of a point at $r=0.1$ to roughly 5–6% at $r=0.7$ under Protocol 4. The two strict-C2 fusion families preserve graceful degradation; the soft-C2 fixed-cardinality family does not.

The Transformer’s structural advantage—query-dependent weighted aggregation across observed views—realizes capability that shared-MLP-then-pool aggregation cannot match within the C1+C2-stable class, validating the empirical capability axis of Theorem 4.1.

Hard-C2 endpoint. DVIMC, evaluated on the same HW 4×4 (protocol, rate) grid, exhibits both predicted hard-C2 failure modes (cross-sample instability and K-Means crash at $|O_i| = 0$); empirical details in Appendix A.3.5. The same canonical CRAFT checkpoint produces ACC in $[79, 97]\%$ on every configuration of the same grid (Table 8) with no crashes.

E Ablation and Sensitivity Details

E.1 Full Ablation Tables

All ablation experiments use 3 seeds and report Protocol 4 ACC (mean \pm std) unless otherwise noted. Each column removes one component from the within-table “Full” reference. All rows use the v4 learnable-placeholder mask strategy to hold mask handling fixed across ablations, so absolute values

Table 16: HandWritten ($V=6$), $r=0.7$. Energy-DIMC retrains per rate (single seed). CRAFT: one canonical attention_mask checkpoint with MFT, 5-seed mean. Bold = best per protocol.

Method	Proto. 1	Proto. 2	Proto. 3	Proto. 4
Energy-DIMC	96.37	95.65	83.98	83.26
CRAFT	97.58 ± 0.9	97.49 ± 0.9	86.03 ± 2.1	85.21 ± 2.4

Table 17: Fusion architecture spectrum on HandWritten ($V=6$): ACC (%) under all four protocols. Bold = best per configuration.

Architecture	r	Proto. 1	Proto. 2	Proto. 3	Proto. 4
Transformer + attn mask (canonical)	0.1	97.28 ± 1.0	97.28 ± 1.0	97.11 ± 1.0	97.14 ± 1.1
	0.3	97.25 ± 1.1	97.26 ± 1.1	95.31 ± 1.6	95.59 ± 1.5
	0.5	97.24 ± 1.1	97.13 ± 1.1	90.02 ± 3.0	90.79 ± 3.0
	0.7	97.24 ± 1.0	97.09 ± 1.1	80.29 ± 5.1	79.06 ± 5.7
SetMLP-Light ($h'=192$)	0.1	94.80 ± 1.3	94.78 ± 1.3	93.83 ± 1.2	94.01 ± 1.2
	0.3	94.54 ± 1.2	94.54 ± 1.3	88.23 ± 1.3	88.82 ± 1.3
	0.5	94.37 ± 1.2	93.94 ± 1.3	78.19 ± 1.6	78.97 ± 1.8
	0.7	94.17 ± 1.2	93.56 ± 1.3	64.38 ± 2.0	62.09 ± 2.3
SetMLP-Match ($h'=560$)	0.1	94.56 ± 1.6	94.53 ± 1.6	92.84 ± 1.5	92.93 ± 1.7
	0.3	93.86 ± 1.6	93.92 ± 1.6	85.30 ± 1.7	85.89 ± 1.7
	0.5	93.45 ± 1.6	93.11 ± 1.6	73.23 ± 1.6	73.83 ± 1.7
	0.7	92.74 ± 1.6	92.19 ± 1.7	57.78 ± 1.9	55.15 ± 1.9
Concat fusion (fixed input, soft C2)	0.1	94.58 ± 0.3	94.53 ± 0.3	93.31 ± 0.3	93.38 ± 0.4
	0.3	94.17 ± 0.2	94.27 ± 0.3	86.13 ± 0.4	86.89 ± 0.2
	0.5	93.98 ± 0.3	93.60 ± 0.4	74.09 ± 0.4	75.04 ± 0.4
	0.7	93.63 ± 0.3	92.93 ± 0.3	58.72 ± 0.6	56.55 ± 0.7

are not directly comparable to the canonical attention-masking results in Table 2; relative ablation pattern is preserved (see Appendix E.4 for mask strategy).

Table 18: Loss and training-stage ablation (Protocol 4 ACC %). Bold = ablation column outperforming Full.

	r	Full	No Stage 2	No Entropy	Recon Only	Repr Only	No Pretrain
HW	0.1	94.23 ± 1.1	94.20 ± 1.0	94.12 ± 1.0	93.66 ± 1.5	16.01 ± 2.4	62.45 ± 3.8
	0.3	87.63 ± 0.9	87.09 ± 0.9	86.96 ± 0.9	86.90 ± 3.8	12.56 ± 0.4	53.56 ± 5.3
	0.5	74.42 ± 1.3	73.62 ± 1.5	73.47 ± 1.6	74.22 ± 5.8	11.33 ± 0.1	43.15 ± 6.4
	0.7	54.27 ± 1.9	53.67 ± 1.9	53.20 ± 1.7	54.83 ± 6.8	10.46 ± 0.1	31.40 ± 4.4
CUB	0.1	76.86 ± 3.7	73.84 ± 1.7	74.26 ± 1.8	79.99 ± 4.8	50.74 ± 3.2	51.80 ± 1.6
	0.3	68.62 ± 4.4	65.63 ± 1.9	66.03 ± 2.1	73.93 ± 4.8	31.60 ± 1.8	49.34 ± 1.3
	0.5	61.54 ± 5.7	57.99 ± 2.5	58.42 ± 2.7	69.28 ± 5.5	15.34 ± 1.1	47.49 ± 3.3

Stage 1 pre-training is essential. Skipping Stage 1 entirely (NO PRETRAIN) drops accuracy by 23–34% on HW and roughly 14% on CUB at the hardest tested rates (Table 18). Stage 1’s role is to learn representations that pre-align with the Stage 2 cluster head; without it, Stage 2 must drive both representation learning and clustering simultaneously, and the clustering objective alone is insufficient under missing-view distributions.

Reconstruction is the load-bearing Stage 1 signal. Replacing Stage 1 with consistency-loss-only training (REPR ONLY, $\lambda_{\text{recon}}=0$) collapses performance to near-random on HW ($\leq 16\%$ on $K=10$, where random is 10%) and to 15–51% on CUB. The reconstruction loss provides the bulk of the cluster-relevant gradient; the consistency loss alone, despite being per-sample and C1-compliant, cannot anchor the representation in the absence of a per-view reconstruction target. This is consistent with the information-theoretic motivation in §5.2: Y is the statistical bridge between views, and per-view reconstruction maximizes a lower bound on $I(h; Y)$ (Proposition B.1).

Consistency loss helps high- V , hurts low- V . Removing the consistency loss (RECON ONLY, $\lambda_{\text{repr}}=0$) leaves accuracy approximately unchanged on HW ($\leq 1\%$ gap to Full at every r) but

improves accuracy on CUB by 3–8% (Table 18). The asymmetry tracks view count: at $V=6$, the SimSiam-style consistency loss reinforces redundant signal across multiple compatible views; at $V=2$ with heterogeneous views, the same loss over-constrains the representation by enforcing alignment between modalities that carry distinct information. Consistency is therefore a dataset-dependent regularizer, not a load-bearing component.

Stage 2 components contribute marginally. Removing the Stage 2 fine-tuning (NO STAGE 2) or its entropy regularizer (NO ENTROPY) reduces accuracy by at most $\sim 3.5\%$ at every condition tested (Table 18). Both are useful but not load-bearing in the C1+C2 sense—they contribute to absolute accuracy without altering the protocol-stable behavior.

MFT helps $V \geq 3$, hurts $V = 2$. Masked fine-tuning (§5.3) yields modest single-digit improvements on HW and MultiFashion at high missing rates and a small degradation on CUB. The asymmetry follows the view-subset ensemble interpretation of MFT (Appendix B.6): at $V \geq 3$, MFT mixes many distinct view subsets and acts as a regularizer; at $V = 2$, only the full-view subset contributes and random view dropping reduces to noise injection.

E.2 Theory-only Core (CRAFT-Core)

CRAFT-Core retains only what Theorem 4.2 mandates—C1 + C2 with attention masking and a Stage 1 reconstruction loss—removing SimSiam consistency, entropy and KL regularizers, MFT, and the Stage 2 cluster-head fine-tuning. A single Core checkpoint per dataset is evaluated under all four protocols at four rates with attention masking applied at inference; Table 19 reports the result. Core escapes the trainability bound at every configuration on both datasets and exceeds every \mathcal{F}_{rec} baseline at every configuration. The gap to canonical CRAFT decomposes into a roughly uniform component on lenient-to-moderate configurations—attributable to the four discarded engineering components collectively—and a regime-dependent component that grows with V and r , reaching $\sim 33\%$ on HW under $V=6$, $r=0.7$, $p_c \rightarrow 0$, where MFT trains the model on the few-view subsets the canonical run encounters at inference.

Table 19: CRAFT-Core ACC (%) on CUB and HandWritten under all four protocols. 3-seed mean \pm std.

Dataset	r	Proto. 1	Proto. 2	Proto. 3	Proto. 4
CUB	0.1	79.96 \pm 3.5	79.79 \pm 3.4	78.36 \pm 2.9	79.01 \pm 3.6
	0.3	76.93 \pm 3.0	77.40 \pm 3.6	73.58 \pm 2.6	72.34 \pm 3.0
	0.5	74.30 \pm 2.9	74.33 \pm 3.0	69.98 \pm 2.6	66.93 \pm 3.2
	0.7	71.47 \pm 2.4	70.91 \pm 2.2	67.19 \pm 2.1	66.93 \pm 3.2
HW	0.1	93.63 \pm 0.9	93.60 \pm 1.0	92.39 \pm 1.6	92.29 \pm 1.7
	0.3	93.35 \pm 1.1	93.27 \pm 1.2	85.08 \pm 2.8	85.46 \pm 3.4
	0.5	92.92 \pm 1.5	92.68 \pm 1.6	71.90 \pm 3.8	72.34 \pm 3.8
	0.7	92.81 \pm 1.8	92.03 \pm 1.7	54.50 \pm 3.3	51.94 \pm 3.2

E.3 Sensitivity Figures

Figure 4 reports the four sweeps at the canonical evaluation point (Protocol 4, $r=0.5$). We re-ran each sweep at $r \in \{0.1, 0.3, 0.7\}$ and confirmed that the optimal settings remain stable: $L=1$ is optimal at every tested missing rate; $d=128$ is optimal for CUB at every rate (larger d overfits on $n=600$); the λ_{repr} dataset-dependence (HW optimum near 0.5, CUB optimum near 0.1) is preserved across rates; temperature τ remains within 0.6% across two orders of magnitude. The relative ordering of configurations in each panel does not change with r , so the canonical configuration in Appendix A.2 is appropriate at all four nominal rates.

E.4 Missing-View Strategy Comparison

In Table 20, the strict-C2 strategy (attention masking) consistently dominates soft-C2 alternatives (learnable, zero, mean), with the gap widening at higher missing rates. This is consistent with Proposition B.2: under attention masking, absent views contribute zero attention weight exactly; under soft-C2, residual leakage of $O(k/(V - k))$ persists and degrades the fused representation.

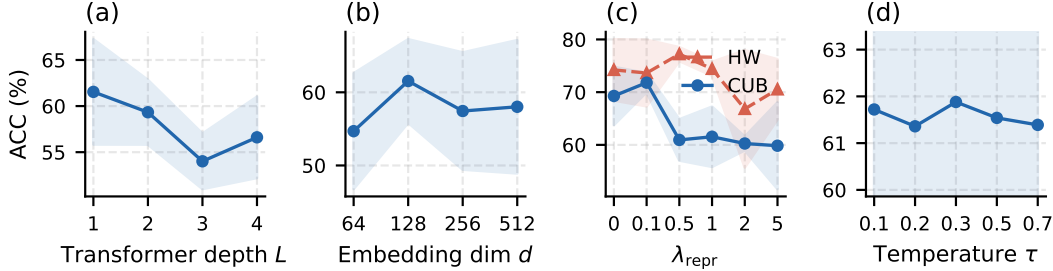


Figure 4: Sensitivity to four key hyperparameters under Protocol 4 $r=0.5$. **(a)** Depth: $L=1$ optimal; deeper fusion amplifies overfitting. **(b)** Embedding dim: $d=128$ optimal for CUB ($n=600$); larger d overfits. **(c)** λ_{repr} : dataset-dependent (HW optimum at 0.5, CUB at 0.1, consistent with the asymmetry in Table 18). **(d)** Temperature: insensitive ($<0.6\%$ spread across two orders of magnitude). Shaded bands: ± 1 std over 3 seeds.

Table 20: Missing-view strategy comparison (CUB, Protocol 4 ACC %). All strategies use the same complete-trained checkpoint; they differ only in how missing-view tokens are handled at inference. Attention masking (canonical CRAFT, strict C2) wins across all rates. Bold = best per row.

r	Attn Mask	Learnable	Zero	Mean
0.1	77.29 ± 4.1	76.86 ± 3.7	76.36 ± 3.4	75.77 ± 2.6
0.3	69.78 ± 5.4	68.62 ± 4.4	66.40 ± 3.3	65.03 ± 0.2
0.5	63.84 ± 7.9	61.54 ± 5.7	58.13 ± 4.4	55.89 ± 0.9

E.5 Aggregation Strategy

Table 21: Aggregation strategy comparison (Protocol 4 ACC %). Bold = best per row.

Dataset	r	CLS	Mean	Max
HW	0.1	94.23 ± 1.1	93.85 ± 0.1	93.45 ± 0.6
	0.3	87.63 ± 0.9	88.72 ± 0.5	84.85 ± 2.1
	0.5	74.42 ± 1.3	75.61 ± 1.5	71.33 ± 3.7
	0.7	54.27 ± 1.9	53.62 ± 2.7	51.69 ± 4.0
CUB	0.1	76.86 ± 3.7	75.50 ± 4.0	76.79 ± 3.0
	0.3	68.62 ± 4.4	68.10 ± 3.7	68.98 ± 3.0
	0.5	61.54 ± 5.7	61.97 ± 4.2	61.92 ± 2.8

In Table 21, the three aggregation strategies (CLS / Mean / Max) cluster within 1–3% of each other, indicating that the C1+C2 properties are carried by the attention mechanism itself, not by the choice of pooling head.

E.6 Attention Analysis

On CUB ($V=2$), with one view missing the learnable placeholder receives approximately 38% of total CLS attention (76% of the uniform share), higher than the 57% ratio observed on HandWritten ($V=6$) because the shorter sequence leaves fewer real tokens to redistribute weight to. Under canonical attention masking, the missing position receives exactly zero weight regardless of the number of views (Proposition B.2, $\varepsilon = -\infty$); Figure 5 visualizes the placeholder attention reallocation pattern on HandWritten as a function of the number of missing views.

F Extended Discussion

F.1 Implications and Practical Recommendations

Cross-view reconstruction modules are not inherently harmful: under the lenient protocols that dominate current IMVC practice, the reconstruction signal implicitly maximizes a lower bound on cluster-relevant information (Appendix B.4) and provides genuinely useful supervision. Our analysis identifies *when* this signal vanishes and *why* the consequence is structural (Theorem 4.2). Three

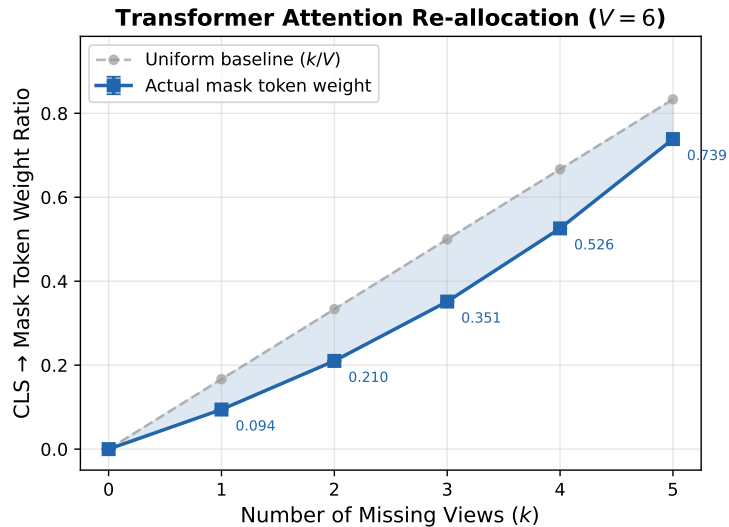


Figure 5: CLS→placeholder attention weight on HandWritten ($V=6$, learnable-placeholder strategy) vs. the number of missing views k . Trained model (solid) vs. uniform baseline k/V (dashed).

practical recommendations follow: IMVC evaluations should report \hat{r} and p_c alongside the nominal missing rate r , without which cross-study comparisons are not meaningful; practitioners deploying \mathcal{F}_{rec} methods on production data should verify $p_c \geq 1\%$ on their target distribution; and future IMVC methods seeking cross-protocol stability should be designed around the C1+C2 conditions of §4, which are structurally required within \mathcal{F}_{rec} and sufficient (under the capability ceiling of Theorem 4.1) outside it.

F.2 Reproducibility Statement

Code, configurations, and a four-protocol evaluation toolkit are released with the paper; CRAFT inference under arbitrary missing-view patterns uses only PyTorch’s standard `MultiheadAttention` key-padding-mask interface, with no custom module required.